DOI:10.1070/RCR4806

Exfoliation of crystals

Leonid A. Aslanov, Sergei F. Dunaev

Faculty of Chemistry, Lomonosov Moscow State University,
Leninskie Gory 1, stroenie 3, 119991 Moscow, Russian Federation

The review is concerned with progress in methods for exfoliation of crystals, from mechanical exfoliation using sticky tape to modern techniques involving sonication-assisted exfoliation, shear exfoliation in liquids using intercalating agents and stabilizers, direct liquid exfoliation and cosolvent exfoliation. The potential of methods of osmotic swelling in water and in organic dispersion media with constant and variable chemical composition of nanosheets, chemical and electrochemical intercalation, exfoliation by hydrazine (including versions resulting in changes in the chemical composition of nanosheets), ionic liquids and supercritical fluids is discussed. Methods for size sorting of nanosheets by density-gradient and cascade centrifugation and the possibility of nanosheet size control are analyzed.
The bibliography includes 136 references.

Contents

1. Introduction 882
2. Mechanical exfoliation 883
3. Liquid-phase exfoliation 884
4. Osmotic swelling 887
5. Chemical and electrochemical intercalation 893
6. Exfoliation by hydrazine 894
7. Exfoliation by ionic liquids 895
8. Exfoliation in supercritical fluids 897
9. Separation and size control of nanosheets 897
10. Conclusion 900

1. Introduction

Exfoliation of crystals involves transformation of layered crystals to a dispersion of single- and few-layer crystalline fragments (2D-nanocrystals). Molybdenum disulfide was exfoliated in 1986,[1] while tantalum disulfide was exfoliated even before that time.[2] Pioneering communications on practical value of exfoliation of crystals date back to the early 1990s.[3,4] At that time, exfoliated layered aluminosilicate minerals (a kind of clays) were used to improve the properties of polymers. For instance, small amounts of exfoliated montmorillonite admixtured to nylon significantly improve the mechanical (including thermomechanical) and fire-retardant properties,[5,6] as well as gas impermeability[7] of the material. Two-dimensional clay nanocrystals improve the properties of not only nylon, but also polyethylene[8] and certain copolymers (in particular, ethylene/vinyl alcohol copolymer).[9] A variety of substances in the form of 0D and 1D nanoparticles were tested as fillers for polymers. Among them, 2D clay nanocrystals appeared to be most efficient taking account of their cost.[10,11]

It was the studies[12] of A.K.Geim and K.S.Novoselov, who were awarded the 2010 Nobel Prize in physics, that gave an impetus to emergence of a new avenue of scientific research, *viz.*, investigation of 2D nanocrystalline state of matter. The merit of Geim and Novoselov is first of all that they demonstrated fundamental differences between the properties of 2D nanocrystals and bulk crystals. This discovery was followed by avalanche-like (Fig. 1) progress in methods of exfoliation of layered crystals and by the development of methods for the synthesis of framework-type 2D nanocrystals that cannot be exfoliated. The term 'nanosheet' was for the first time used by Sasaki *et al.*[13] An increase in the number of publications devoted to exfoliation of crystals was accompanied by qualitative changes. Namely, pioneering studies in this field were carried out with graphene

L.A.Aslanov. Doctor of Chemical Sciences, Professor, Head of Laboratory of Structural Chemistry at the Faculty of Chemistry, MSU. Telephone: +7 (495)939 – 1327, e-mail: aslanov@struct.chem.msu.ru
Current research interests: structural chemistry.
S.F.Dunaev. Doctor of Chemical Sciences, Professor, Head of Division of General Chemistry at the Faculty of Chemistry, MSU.
Telephone: +7 (495)939 – 1596, e-mail: dunaev@general.chem.msu.ru
Current research interests: hybrid, composite and dispersion-reinforced materials, fibre/matrix composite materials, methods of their synthesis and chemical compatibility.

Received 19 December 2017
Translation: A.M.Raevskiy

© 2018 Uspekhi Khimii, Russian Academy of Sciences and Turpion Ltd.

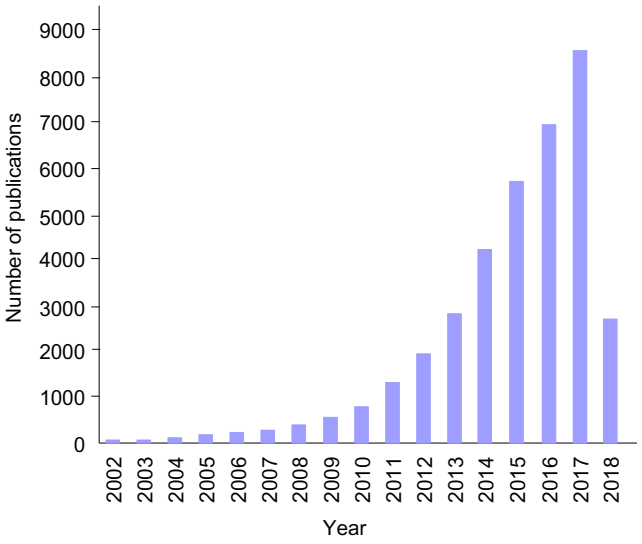


Figure 1. Annual number of scientific publications devoted to nanosheets and reported between 2002 and 2018.
Data analysis was performed using the Web of Science database with the term 'nanosheet'. Publications of 2018: the first quarter is covered.

nanosheets prepared using Scotch tape. A decade later, the focus was shifted towards mass production of nanosheets and nanosheet size control using production lines (see below).

Two-dimensional nanocrystals have a great potential for practical application in, *e.g.*, electronics. In the last few decades the number of transistors on silicon chips doubled every 24 months.[14] Eventually, miniaturization of silicon-based transistors will lead to a limit. This will be followed by overheating of electronic components and an increase in production cost. In this connection, 2D nanocrystals of certain compounds are candidates for being used instead of silicon. Two-dimensional nanocrystals of transition metal dihalcogenides (TMD)[15–17] and black phosphorus (phosphorene)[18–20] are treated as promising semiconductors, while hexagonal boron nitride (h-BN) is thought to be used as dielectric.[21] These compounds can form a basis for spintronics.[22,23] 2D-Nanocrystals can be used as sensors,[24,25] catalysts[26] (in particular, photocatalysts),[27] luminophores,[28] materials for bioimaging[29] and components of solar cells,[30] electrode materials for batteries[31,32] or supercapacitors,[33,34] as well as lubricants.[35] They are suitable for production of inks to print electronic circuits,[36] photodetectors[37] and materials for bone surgery.[38]

Among a variety of reviews on the properties of nanosheets of certain substances published in the last decade (see, *e.g.*, Refs 39–43; as far as we know, no reviews written in Russian are available), there are no summary reviews concerning methods of exfoliation. Here, we compare methods for fabrication of 2D nanocrystals and consider the results of studies carried out in the last 15 years, *i.e.*, the period of rapid progress in this new branch of chemistry. Various physical properties of 2D nanocrystals are left out of consideration because the authors decided to dwell on chemical aspects of exfoliation processes, which are at least as versatile as methods of synthesis considered in our recent review.[44]

2. Mechanical exfoliation

By mechanical exfoliation is usually meant delamination of layered crystals using sticky tape. The method became popular since the experiments by A.K.Geim and K.S.Novoselov,[12] who used this technique to prepare graphene and studied the properties of the material. Mechanical exfoliation still remains the simplest and most reliable method for preparation of nanosheets with different number of layers including single-layer ones. 'Reliability' means that the chemical composition of the exfoliated layers remains unchanged. For instance, graphite can be exfoliated by oxidation and subsequent reduction; however, the chemical composition, structure and properties of graphene thus obtained differ from those of graphene prepared by mechanical exfoliation.

Information is scarce about mechanical exfoliation. Usually, the authors of studies on the properties of 2D nanocrystals simply mention that the systems in question were obtained by mechanical exfoliation and then discuss the results of experiments. Mechanical exfoliation as a process involves a number of steps.[45] Typically, in the first step few-layer crystals of, *e.g.*, MoS_2 are peeled off using adhesive Scotch tape. Then, the freshly cleaved thin crystals are brought into contact with a substrate chosen by the experimentalist and rubbed to further cleave them. As the Scotch tape is removed, nanocrystals with different number of layers are left on the substrate and the necessary nanocrystals are picked up.

Mechanical exfoliation does not necessarily use Scotch tape. Single crystals of $TaSe_2$ with millimetre-length lateral size were mechanically exfoliated[46] using two substrates, one of them being coated with nonadhesive viscoelastic layer of poly(dimethylsiloxane) (PDMS). The surface of the substrate containing $TaSe_2$ crystals was pressed against the other PDMS-coated substrate and peeled off. This operation was repeated until atomically thin $TaSe_2$ flakes were observed on the PDMS surface. These nanocrystals were transferred to the surface of an SiO_2/Si wafer and then studied. The advantage of the PDMS surface over Scotch tape is that it leaves no adhesive traces on the wafer surface preventing the motion of the cantilever of an atomic force microscope (AFM). Although the authors[46] stated that both methods allow one to prepare nanosheets of the same thickness and lateral size, experiments showed that the nanosheets were 5 to 15 layers thick and did not include single- or bilayer nanosheets.

In another study[47] TiS_3 crystals were picked up using a viscoelastic stamp (Gelfilm from Gelpak), the stamp with TiS_3 material was placed on a SiO_2/Si substrate and slowly peeled off leaving TiS_3 crystals exfoliated to one or another extent on the substrate surface. Yet another viscoelastic stamp was used for further mechanical exfoliation of the crystals and removal of undesired nanoflakes.

Large-area nanosheets are prepared from large crystals preliminarily grown using specific methods. For instance, large tin disulfide crystals (lateral size of up to 5 mm, thickness of hundreds of micrometres, growth steps of hundreds of nanometres) were synthesized[48]

using vapour-phase transport method. To a mixture of tin and sulfur, iodine was added to provide vapour-phase transport of tin (as a result of formation of volatile tin iodide). Silver sulfide was used as catalyst. A sealed tube was heated at 750 °C for 7 to 28 days (temperature gradient along the tube was 50 °C).[48] As a result, crystals of the 2H-SnS_2 polytype were grown (this is one of more than 20 known tin disulfide polytypes).[49–51] Then, mechanical exfoliation (Scotch tape) was done, followed by transfer of nanosheets to SiO_2/Si wafers. The thinnest nanosheet prepared by one-step exfoliation was 10 nm thick (according to AFM data), which corresponded to 20 SnS_2 layers.

Specific methods for growth of large crystals are usually employed to provide conditions for the most accurate studies on the properties of nanosheets. For instance, tin disulfide (see above) can be used in optoelectronics. The SnS_2 bandgap varies from 1.82 to 2.41 eV depending on the crystal structure (polytype), method of synthesis and defect type and concentration. Vanadium-doped 4H-SnS_2 is a promising material for fabrication of solar cell components. Doping produces an impurity level in the bandgap of SnS_2 and the material can now absorb not only high-energy, but also low-energy photons.[52]

Mechanical exfoliation can be performed with testers used in the studies of tribological properties of substances. For instance, a study on tribological properties of $NbTe_2$ was accompanied by exfoliation of the material through ball milling. Exfoliation was detected by scanning electron microscopy (SEM) and X-ray powder diffraction.[53]

A study[54] on exfoliation of MoS_2 crystals in the course of milling in a ball mill revealed that the lateral size of MoS_2 nanosheets decreases with increasing the milling time. The defectiveness of nanosheets increases with increasing the milling time and the ball/powder mass ratio. Simultaneous exfoliation and functionalization of the surface of nanosheets with sorbents in the course of mechanical grinding of graphite-like carbon nitride was reported.[55]

From a brief survey of mechanical exfoliation it follows that preparation of single-layer 2D nanocrystals is a complicated, low-yield process. Therefore, it is not surprising that most often crystals are exfoliated using other methods, *e.g.*, liquid-phase exfoliation.

3. Liquid-phase exfoliation

3.1. General

Liquid-phase exfoliation requires:

— energy expenditure to overcome interlayer attraction between adjacent sheets in the crystal;

— stabilization of nanosheets against re-aggregation by using appropriate solvent or surfactant; and

— size selection of nanosheets since usually they are characterized by certain thickness and lateral size distributions (single-layer nanosheets are rare to form).[56]

Typically, the starting crystals are ground and mixed with a dispersion medium, *i.e.*, an individual liquid substance or aqueous solution of a surfactant or polymer, and the mixture is subjected to sonication or mechanical dispersion in a mixer for a few hours or a longer period of time. Then, the dispersions are centrifuged at low rotation speed to remove unexfoliated coarse-crystalline material, while the dispersion containing partially or completely exfoliated crystals, that is, nanosheets of different thickness and lateral size is fractionated.[56]

Carrying out exfoliation, one should take account of the fact that the efficiency of the process depends on certain parameters. These include the surface tension difference between the dispersion medium and the crystals being dispersed, the concentration of the stabilizer (surfactant or polymer), the concentration of crystals being dispersed, the duration of ultrasonic treatment and the volume of the dispersion being treated, power output of ultrasonic generator and efficiency of acoustic contact or the mixer speed, temperature (elevated temperature of the dispersion medium can cause chemical degradation of nanosheets, *e.g.*, partial hydrolysis of chalcogenides in water).[56]

So-called direct liquid exfoliation is performed using specially selected liquids.[57–66] This is an attractive process since it uses no intercalating agents and therefore the resulting 2D nanocrystals contain no impurities. To choose the dispersion medium properly, it is useful to compare the surface tension of a liquid and the substance to be exfoliated. It is even better to divide the surface tension into two components, a polar and a dispersive one. A properly chosen dispersion medium should have the surface tension similar to that of the crystals to be exfoliated and the same polar to dispersive component ratio as that of the exfoliated crystals.[67]

Recently, exfoliation has been achieved using mixtures of liquids that are commonly used in preparative-scale laboratory practice.[68–74] Such mixtures have fairly obvious advantages, namely:

— by varying the mixture component ratios one can more readily choose the surface tension of the liquid phase;

— utilizing mixtures allows one to exclude toxic components;

— mixtures of cheap components can be used instead of expensive individual dispersion media;

— the use of mixtures considerably extends the number of solvents for exfoliation.

Unfortunately, the yield of single-layer nanosheets prepared by liquid-phase exfoliation is low. Information regarding the ease of exfoliation[75] is scarce and requires verification.

3.2. Sonication-assisted exfoliation

There are two kinds of liquid-phase sonication-assisted exfoliation, *viz.*, bath sonication and tip sonication. Ultrasonic waves generate shear deformations and cavitation bubbles, which collapse to break up the layered structure crystal and produce single- or few-layer nanosheets. The surface tension at the crystal/liquid interface is of great importance when a bulk layered crystal is immersed in a liquid. The interaction between a specially chosen liquid and the crystal surface can be stronger than van der Waals attraction between adjacent nanosheets and thus stabilize the dispersion.[76]

Generally, the smaller (closer to zero) the change in the enthaply of mixing of the dispersed phase and dispersion medium per unit volume the easier the exfoliation process. If the surface energy of the dispersed phase

matches that of dispersion medium, the energy expenditure for exfoliation is negligible. Therefore, exfoliation of crystals requires individual selection of appropriate dispersion medium.[62]

Longer sonication times of dispersions lead to higher concentrations of nanosheets, but their dimensions decrease in inverse proportion to the square root of time; in addition, defects are induced, mainly originating from edge effects.[76] To improve the efficiency of sonication-assisted exfoliation, admixtures are added to the dispersion. For instance, exfoliation of MoS_2 was carried out in ethanol in the presence of pyrene;[77] treatment of the dispersion for 45 h gave 8% of single-layer nanosheets, while the maximum in the nanosheet thickness distribution indicated that nanosheets five monolayers thick were the major product. Pyrene additive played a dual role, namely, it facilitated exfoliation and stabilized the dispersion of MoS_2 nanosheets. Yet another example is as follows: sonication-assisted exfoliation of hexagonal boron nitride in a dispersion was a slow, low-yield process that took tens of hours;[78] however, simultaneous functionalization of the surface of h-BN nanosheets with amines and other molecules that form donor-acceptor bonds with unoccupied orbitals of boron atoms, as well as stabilization of h-BN nanosheets with surfactants or a nickel phthalocyanine complex significantly accelerated the process.

Of course, liquid-phase sonication-assisted exfoliation has certain disadvantages. First, particles of the dispersed phase are characterized by broad thickness and lateral size distributions. Next, the yield of the process is low.[76] The yield of single-layer particles is a few per cent (*cf.* 90% for electrochemical exfoliation of lithium-intercalated crystals, see below). Besides, the smaller the thickness of 2D nanocrystals the smaller their lateral size.

3.3. Shear exfoliation

Shear exfoliation of crystals can be achieved using a blender. An example is provided by exfoliation of MoS_2 crystals in water containing dissolved sodium cholate (a surfactant) at a maximum rotor speed of 8335 rpm.[66] The set of controlled parameters included the crystalline MoS_2 concentration (C_{MoS_2}), the surfactant concentration (C_{surf}), the mixing time (t), the liquid volume (V) and the rotor speed (N). It was found that the rotor diameter affects the outcome, but this was a fixed parameter in that study. Mixing experiments were carried out using the following standard parameters determined after preliminary trials: $C_{MoS_2} = 50$ mg ml^{-1}, $C_{surf} = 10$ mg ml^{-1}, $t = 120$ min, $V = 1000$ ml at the maximum rotor speed N. The dispersion was centrifuged at 1500 rpm (240 g) for 90 min to remove unexfoliated crystals. The top 50% of the supernatant was collected for analysis.

A transmission electron microscopy (TEM) analysis revealed nanosheets with length of 85 nm (averaged over 100 nanosheets) and width nearly half the length. According to AFM data, the average thickness of MoS_2 nanosheets expressed as the number of layers per nanosheet is 4.6. Molybdenum disulfide nanosheets covered with the surfactant have electrical double layers that prevented aggregation of nanosheets. The concentration C_{surf} has a strong effect on exfoliation outcome, which is characteristic of not only MoS_2, but also graphene.[79]

Empirical dependence of the exfoliation yield Y ($Y = C : C_{MoS_2}$, where C is the concentration of MoS_2 nanosheets) has the form[66]

$$Y = \left(14\,C_{surf}^{-0.8} + 0.14\,C_{surf}^{1.4}\right)^{-1} \quad (1)$$

As C_{surf} increases, the yield increases to a limiting value corresponding to saturation of the nanosheet surface with surfactant molecules. This is the so-called critical micelle concentration (CMC). Then, the yield decreases with increasing C_{surf}. Equation (1) is not universal, *viz.*, the yield of graphene depends on the $C_{surf} : C_{gr}$ ratio rather than C_{surf}.[79] However, the length and thickness of MoS_2 nanosheets depend only on C_{surf} and reach maximum values of 200 – 250 nm and 10 layers, respectively, at $C_{surf} \approx 2$ mg ml^{-1}. At $C_{surf} = 30$ mg ml^{-1}, the thickness and length of MoS_2 nanosheets decrease to 2 layers and 40 nm, respectively, thus demonstrating a correlation.[66]

To understand the correlation between the yield and surfactant concentration, the zeta-potential was plotted *vs.* C_{surf} at fixed C_{MoS_2}. The plot is very similar to the dependence of the exfoliation yield on C_{surf}. First, the zeta-potential increases with increasing surfactant concentration, reaches a maximum value at CMC and then decreases. At $C_{surf} <$ CMC, the coverage of nanosheets with surfactant molecules increases and reaches the limiting value at CMC. The maximum zeta-potential corresponds to the highest inter-micelle repulsive barrier. As the surfactant concentration in the dispersion further increases, surfactant molecules form micelles without crystalline core comprised of nanosheets. This leads to coagulation of nanosheets, which becomes more intense as the surfactant concentration increases. Coagulation is due to the fact that the surfactant concentration in solution exceeds that in interlayer regions of the crystal and to a decrease in osmotic pressure in the interlayer space between nanosheets.

The concentration of MoS_2 nanosheets in the aqueous dispersion depends almost linearly on the exfoliation time, namely, $C \sim t^{0.88}$ (however, the length and thickness of nanosheets demonstrate no dependence on time).[66] The concentration of MoS_2 nanosheets in the aqueous dispersion is proportional to $C_{MoS_2}^{1.25}$ and to the rotor speed. However, the shape of the dependence on the rotor speed is governed by the blender design.[65] The concentration of nanosheets in the dispersion decreases as the liquid volume in the blender increases: $C \sim V^{-0.41}$.[66]

3.4. The choice of the medium

The choice of the dispersion medium is crucial to successful exfoliation. It depends on the nature of the dispersed phase and on the goal of exfoliation. For instance, MoO_3 and black phosphorus are chemically unstable in water and rapidly degrade; therefore, non-aqueous solvents should be used as dispersion media. Also, it is often difficult to remove surfactant from aqueous dispersion of nanosheets after exfoliation. This is usually achieved by dialysis; however, a decrease in the surfactant concentration can lead to aggregation of nanosheets. Aqueous dispersions are stabilized using polymers including proteins; however, this reduces the

extent of exfoliation and complicates the size and thickness selection of nanosheets. Stable dispersion can be prepared in, *e.g.*, *N*,*N*-dimethylformamide (DMF), dimethyl sulfoxide, isopropyl alcohol and *N*-methyl-2-pyrrolidone. The surface tension values of these liquids are close to those of many crystals to be exfoliated, so the changes in the enthalpy during exfoliation are minimum.[56]

It is recommended to carry out a two-step exfoliation process. The first, short-term step is necessary to purify the dispersed phase. The second step takes nearly five times longer time and involves exfoliation of crystals *per se*. The first step is followed by centrifugation to remove the dispersion medium and impurities. Two-step exfoliation is especially necessary when using ionogenic surfactants since often one deals with ionic impurities that shield the surfactant charge and reduce the surfactant activity. As the concentration of the dispersed phase increases (>30 g litre^{-1}), the concentration of exfoliated nanosheets also increases.[56]

Typically, exfoliation in organic media requires long-term sonication and is characterized by low yield. When the starting MoS_2 crystals were pretreated with aqueous solution of an inorganic salt that intercalated into MoS_2 upon evaporation of water, the exfoliation time shortened nearly 100-fold and the yield increased by a factor of 32. These crystals exfoliated with ease in an organic solvent. A total of 65% of the dispersed phase were 1 to 5 layers molybdenum disulfide nanosheets.[80, 81]

If the surface tension of the dispersed phase and organic dispersion media differ considerably, one should use aqueous solutions of surfactants, *e.g.*, sodium cholate, sodium dodecyl benzylsulfonate, cetyltrimethylammonium dodecyl sulfate (anionic surfactants) or cetyltrimethylammonium bromide (cationic surfactant); nonionogenic surfactants are also utilized. Stable dispersions can be prepared if the surfactant concentration is maintained below the CMC, *e.g.*, 5 g of sodium cholate in 1 litre of water. The size and thickness of nanosheets depend on the surfactant concentration to a greater extent compared to other parameters of the system in hand.[56]

3.5. Exfoliation conditions: the choice

Methods of sonication of dispersions, that is, bath sonication and tip sonication, influence exfoliation of different crystalline substances in different manner. For instance, graphite can be exfoliated using both methods, while the maximum yield of large-area TMD nanosheets is obtained only in the latter case. Contrary to this, the most appropriate method for exfoliation of GaS is bath sonication. Therefore, not only the dispersion medium, but also conditions for sonication-assisted exfoliation should be chosen properly.

It is commonly accepted[56] that tip sonication of dispersions of different chemical composition is more efficient than bath sonication due to the higher rate of the process. Namely, tip sonication of a dispersion containing $30-50$ g litre^{-1} of crystals for less than 24 h results in a dispersion of nanosheets with a concentration of 1 g litre^{-1}. It is appropriate to use the operating mode with an ultrasonic generator power output of ~ 300 W since the quality of exfoliation reduces at lower power, whereas at higher power output one deals with faults due to the long exfoliation time. Typically, sonication takes 5 to 7 h. It is crucially important to preclude heating of the sample. Experience showed that at high loads the surface of the sonic probe should be replaced periodically. Besides, the probe should be exchanged every $3-5$ months. Otherwise, the yield of exfoliated nanosheets decreases.[56]

Experience showed that two-step sonication is preferable for such layered materials, as WS_2. First, a dispersion of WS_2 in aqueous surfactant solution (6 g litre^{-1}) was exfoliated for 1 h using pulsed sonication (flathead probe tip, pulse duration 6 s, off time 2 s). Then, the dispersion was centrifuged at 5000 rpm for 1.5 h, the supernatant was decanted, an aqueous surfactant solution (2 g litre^{-1}) was added to the sediment and the dispersion was sonicated for an additional 5 h, all other things being equal. Two-step sonication-assisted exfoliation allows one to increase the yield of nanosheets and to remove impurities.[82]

Ultrasonic bath exfoliation takes longer time and requires greater energy expenditure, being less reproducible compared to the process assisted by tip sonication. The cheapest method to prepare dispersions of nanosheets is to use a mixer. The yield of exfoliated material is independent of the liquid volume and therefore the method can be implemented on a large scale. It is also suitable for exfoliation of graphite; however, TMD crystals break up in this case, the concentration of large-area nanosheets is low and one should use sonication.[56]

3.6. Characterization of samples

UV/Vis absorption spectroscopy is of great importance when analyzing dispersions of nanosheets, although the method is often underestimated. First, it provides information on the structure of exfoliated nanosheets since data on excitonic transitions characteristic of crystals of inorganic salts, their polytypes and polymorphs are well documented. Next, the concentrations of substances can be determined. Note that this can be done in the transmission rather than absorption mode because the results of measurements contain information related to both absorbance and scattering of light by nanosheets. The scattering component of the extinction coefficient and the absorption coefficient are size-dependent[56] due to edge and confinement effects (see †).

Changes in the electronic energy band structure of layered materials as a result of edge and confinement effects are reflected in changes in the magnitude and position of excitonic transitions. Therefore, it is expected that optical exciton spectra will change depending on the lateral size and thickness of nanosheets.[56] Next, Raman spectroscopy provides information on the lattice vibrations in crystals and, therefore, on the crystal structure. The method allows one to verify whether the exfoliated material is structurally similar to the starting (bulk) crystalline phase, *i.e.*, to determine the amount of defects introduced into the nanosheets. Since the surface area of the Raman spot is very small, the results of measure-

† The quantum confinement effect, *i.e.*, an increase in the bandgap of a semiconductor, manifests itself if the thickness of the nanosheet is less than the exciton Bohr radius.

ments can vary from spot to spot, so averaging over tens of measurements is required.[56]

In addition to analysis of the Raman modes, Raman spectrometers can be used to measure luminescence. This is particularly important for, *e.g.*, TMD since bulk TMD crystals are non-direct gap semiconductors, whereas single-layer nanosheets are direct-gap semiconductors and thus exhibit luminescence. By measuring the luminescence intensity one can determine the amount of the exfoliated material. The ratio of the photoluminescence intensity to the fundamental Raman mode intensity is a measure of the content of single-layer nanosheets in the dispersion.[56] When recording Raman spectra, experiments should be carried out in liquid dispersions at minimum laser power to avoid aggregation of nanosheets and heating of samples.

4. Osmotic swelling

Exfoliation of layered crystals through adsorption of water in the interlayer regions is called osmotic swelling. There are two types of swelling, intracrystalline and osmotic. In the former case, the interlayer distances in crystals increase due to hydration of interlayer structural units and arrangement of water molecules in ordered fixed crystallographic positions. Intracrystalline swelling is typical of clays, layered double hydroxides (LDH) and some other substances. Osmotic swelling assumes filling the interlayer space in the crystal with large amount of water from the dispersion medium and transformation of the crystal into a colloidal system. Osmotic swelling is an important method for exfoliation of crystals if other methods are unsuitable.[83, 84]

Hydrophilic layered crystals comprised of alternating anionic nanosheets and alkali metals cations sandwiched between them can be exfoliated by osmotic swelling. The method offers advantages over sonication-assisted or shear and mechanical exfoliation of crystals since it produces single-layer nanosheets in higher yield. The technique is simple. The replacement of alkali metal ions by bulky cations, *e.g.*, tetraalkylammonium makes the interlayer space in crystals accessible to water molecules due to the large size of the cations.

The replacement of alkali metal cations by tetraalkylammonium ions using a minimum amount of the latter causes the electrolyte concentration in the dispersion medium to be much lower than in the interlayer regions. This will produce osmotic pressure and subsequent inflow of water to the interlayer layers of crystals, thus providing conditions for osmotic swelling of the crystals. The interlayer distances in the crystal can increase hugely (Fig. 2). Eventually, exfoliation of crystals occurs. Lateral dimensions of nanosheets thus prepared are of the order of a few micrometres.

Exfoliation of crystals by osmotic swelling is achieved using aqueous solutions of amines, especially, 2-(dimethylamino)ethanol (DMAE).[83]

The efficiency of osmotic swelling can be illustrated by certain examples. Single crystals $K_{0.8}[Ti_{1.2}Fe_{0.8}]O_4$ were flux grown[85] from the reaction mixture of the $TiO_2 : Fe_2O_3 : K_2CO_3 : MoO_3 = 1.2 : 0.4 : 2.03 : 1.63$ composition. After calcination the solvent (potassium molybdate) was removed with water, the crystals were isolated by filtration and protonated by stirring in 0.5 M HCl at room temperature for 2 days. The acid was replaced after 24 h to ensure complete ion exchange. Finally, the process resulted in the $H_{0.8}[Ti_{1.2}Fe_{0.8}]O_4 \cdot H_2O$ crystals.

To study osmotic swelling, 0.2 g of $H_{0.8}[Ti_{1.2}Fe_{0.8}]O_4 \cdot H_2O$ crystals were mixed with 100 ml of aqueous solutions of amines or tetraalkylammonium hydroxides, which acted as intercalating agents. The concentrations of the amine or tetraalkylammonium hydroxide solutions were expressed as the ratio of the amount of amine or tetraalkylammonium hydroxide to

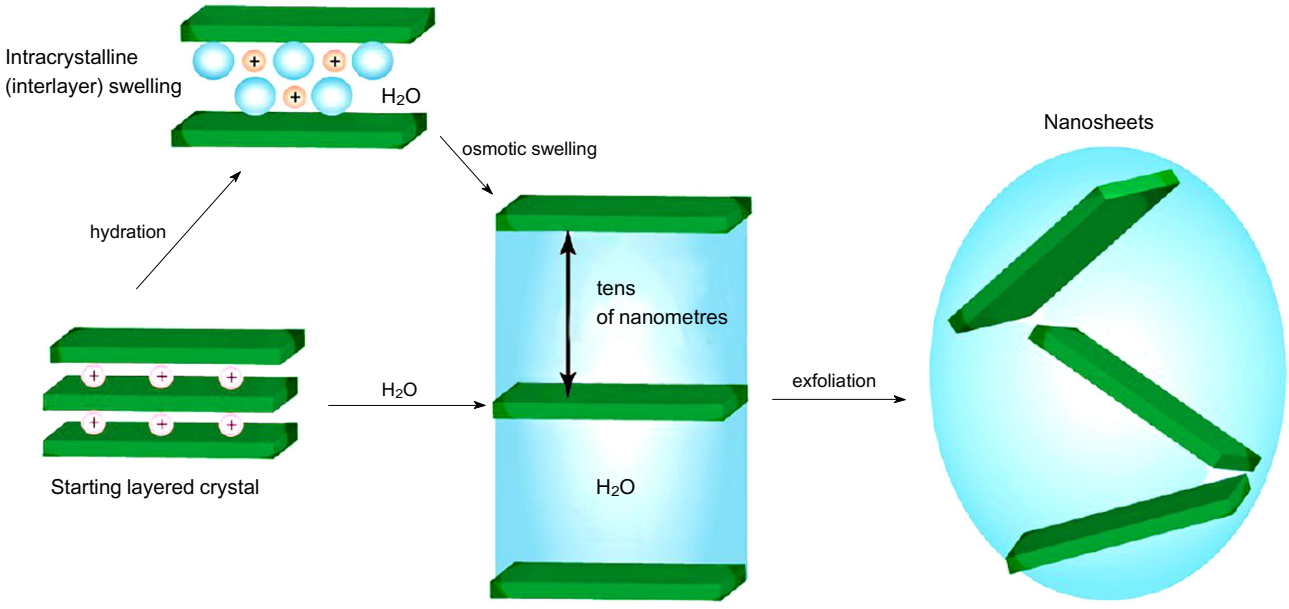


Figure 2. Osmotic swelling and exfoliation of layered crystal: a schematic.[85]

the cation exchange capacity of the protonated titanate crystals (0.8 mol per formula unit) — $N:H^+$. The ratio $N:H^+ = 1$ corresponds to an absolute concentration of ammonium hydroxides of 0.00865 mol litre^{-1}. The mixture was allowed to stay for 24 h. The amount of amine or tetraalkylammonium hydroxide was determined by titration with hydrochloric acid. The amount of intercalated ammonium ions was calculated by subtracting the equilibrated amount of amine (ammonium) in the supernatant after swelling from the amount of amine (ammonium) in the starting solution before swelling. Then, the concentration of amine (ammonium) in the interlayer space of the swollen crystals was calculated (the corresponding volume of water inflow was obtained by multiplying the sheet surface area in the crystals by the expanded interlayer distances that were determined by X-ray diffraction) and the concentration difference between the interlayer space and the solution was found.

When the $H_{0.8}[Ti_{1.2}Fe_{0.8}]O_4 \cdot H_2O$ crystals were dispersed in DMAE solution, an increase in the sample volume, or crystal swelling, was observed immediately. The degree of swelling was dependent on the solution concentration. The maximum swelling was achieved at $N:H^+ = 0.5$; the interlayer distances increased by a factor of 100. The extent of swelling in dilute solutions increased almost linearly with increasing DMAE concentration. Note that it was impossible to achieve homogeneous swelling at small $N:H^+$ ratios (*e.g.*, $N:H^+ = 0.1$). The swollen crystals had iridescent colours observed by optical microscopy and diffuse diffraction patterns were detected by small-angle X-ray scattering (SAXS). The degree of swelling decreased at $N:H^+ > 0.5$. For instance, the interlayer distance equal to 90 nm at $N:H^+ = 0.5$ shortened to 68 nm at $N:H^+ = 1$. As the $N:H^+$ ratio further increased, the extent of swelling continued to decrease, although in a lowed fashion (Fig. 3). At very high amine concentrations in the dispersion, swelling became almost indistinguishable.[85]

The interaction between acidic protons in the crystals and DMAE results in $[(DMAE)H]^+$ cations that intercalate into the interlayer space of crystals. Thus, the reaction system contains two types of $[(DMAE)H]^+$ cations, intracrystalline and those present in solution (external cations). It was found that at $N:H^+ < 0.5$, external cations $[(DMAE)H]^+$ intercalate into the crystals along with a fixed amount of water molecules and thus ensure an almost linear increase in the interlayer distances in the crystal. The concentration of $[(DMAE)H]^+$ in the interlayer space is nearly constant (0.04 mol litre^{-1}), being negligible outside the crystals. An increase in the initial concentration of DMAE above $N:H^+ = 0.5$ causes no $[(DMAE)H]^+$ intercalation into the crystal owing to complete neutralization of hydrogen ions, but water inflow into the crystal decreases due to an increase in the concentration of $[(DMAE)H]^+$ ions in the solution. At $N:H^+ = 10$, the concentration of DMAE in the crystal is nearly equal to that in the solution. All tertiary amines provide an identical extent of swelling with a maximum at $N:H^+ = 0.5$. The maximum swelling achieved with all quaternary ammonium bases was observed at $N:H^+ = 0.3$.[85]

Protonated crystals $H_{0.8}[Ti_{1.2}Fe_{0.8}]O_4 \cdot H_2O$ were mixed with not only DMAE solutions, but also tetrabutylphosphonium (TBP^+) hydroxide solutions of different

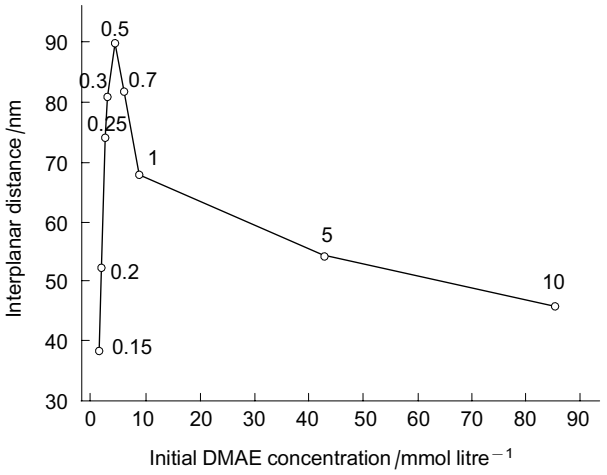


Figure 3. Expanded interlayer distance plotted *vs.* initial DMAE concentration.[85]
Number near the curve denote the $N:H^+$ ratios.

concentrations from 0.1- to 10-fold excess of the ion exchange capacity of $H_{0.8}[Ti_{1.2}Fe_{0.8}]O_4 \cdot H_2O$. The mixture was allowed to stay overnight. The maximum swelling of crystals was observed at $TBP^+:H^+ = 0.3$; however, the largest nanosheet dimensions were found at $TBP^+:H^+ = 0.5-10$, which is probably indicative of fragmentation of nanosheets at small amounts of tetrabutylphosphonium in solutions. At $TBP^+:H^+ = 0.3$, the interlayer distances in the swollen crystals were as long as 85 nm, whereas no swelling was observed at $TBP^+:H^+ = 0.1-0.2$. The interlayer distances are inversely proportional to the square root of the molar concentration of tetrabutylphosphonium hydroxide, which is consistent with the idea that micelles are stabilized by the electrical double layer. Shaking the swollen crystals in electrolyte solution after 1–2 h led to formation of a dispersion that was stable over a period of a few weeks. The nanosheets were 1.3 nm thick and their lateral dimensions spanned the range from a few hundreds of nanometres to a few micrometres.[85,86]

Swelling as a process exhibits no dependence on the amine composition, being strongly dependent on the molar concentration of electrolyte. The amount of intercalated substance depends on the acid-base relationships, while water inflow into the interlayer space of the crystal is always governed by the concentration equilibrium between the interlayer space and external solution.[83]

Exfoliation of titanates using osmotic swelling has been extensively studied (see, *e.g.*, Refs 84, 87, 88). We will dwell on yet another telling example, *viz.*, a study[84] on protonated form, $H_{4x/3}Ti_{2-x/3}O_4 \cdot H_2O$ ($x = 0.8$), prepared by acid treatment (1 M HCl, 3 cycles) of $K_xTi_{2-x/3}Li_{x/3}O_4$ crystals obtained by high-temperature solid-phase synthesis from a mixture of K_2CO_3, Li_2CO_3, and TiO_2. Weighed amounts (0.4 g) of the protonated form of the titanate were treated with aqueous solutions (100 ml) of tetramethylammonium (TMA^+) hydroxide or tetrabutylammonium (TBA^+) hydroxide at TMA^+ (in solution)/H^+(in crystals) mole ratios from 0.5 to 50 and $TBA^+:H^+$ mole ratios from 0.5 to 15. The mixtures were

mechanically shaken (180 times per minute) for seven days or manually shaken (200 times a day) for 18 weeks.

At $TMA^+:H^+ = 0.5-4$, the X-ray diffraction pattern of the solid sediment obtained after centrifugation of the dispersion represented a broad halo, thus indicating the absence of the long-range order and exfoliation of the sample. At $TMA^+:H^+ = 5-50$, the X-ray diffraction pattern exhibited a series of peaks progressively shifted towards small scattering angles as the $TMA^+:H^+$ ratio decreased. All peaks were indexed to $0k0$. The intersheet spacing (d) in the crystals was 9.2, 5.8, 4.8, 4.0 and 2.6 nm at $TMA^+:H^+ = 5$, 10, 15, 20 and 50, respectively, which corresponds to an expansion of about 3 to 10 times compared to $d \approx 0.92$ nm in the starting $H_{4x/3}Ti_{2-x/3}O_4 \cdot H_2O$ ($x = 0.8$) due to osmotic swelling. Small widths of X-ray diffraction peaks at large $TMA^+:H^+$ ratios were indicative of ordered structure of the crystal of the osmotically swollen phase. However, the diffraction peaks broadened as the $TMA^+:H^+$ ratios decreased.[84]

Systems containing TBA^+ demonstrated qualitatively similar behaviour. Experiments using SAXS confirmed the results of observations. Further discussion was held considering the intersheet spacings determined by SAXS because the results of measurements were insensitive to centrifugation. It was found[84] that the degree of osmotic swelling is inversely proportional to the square root of the molar concentration of electrolyte. The dimensions of nanosheets were determined by different parameters. The lateral size of nanosheets isolated from dispersions prepared by mechanically shaking solutions containing crystals and ammonium cations was dependent on the $TBA^+:H^+$ ratio (0.2–0.4, 3 and 7 μm at $TBA^+:H^+ = 0.5-5$, 10 and 15, respectively), being about 8 μm regardless the $TMA^+:H^+$ ratio. In the case of manual shaking the lateral size was ~8 μm for both cations.[84] Dispersions of nanosheets prepared by exfoliation in the presence of TBA^+ cations were more stable when contained small rather than large nanosheets. The stability of dispersions prepared by exfoliation in the presence of TMA^+ cations was nanosheet size independent.

An analysis of dispersions using a polarization microscope revealed a nematic liquid-crystalline phase in the sample prepared by mechanical shaking at $TMA^+:H^+ = 0.5$. This indicated an anisotropic distribution of nanosheets in the dispersion. Dispersions prepared by manual shaking at $TBA^+:H^+ = 0.5$ or 2 also demonstrated liquid-crystalline behaviour. It was found that the liquid-crystalline state depends on the concentration and lateral size of nanosheets, namely, the smaller the size the higher the concentration.[84]

The thickness of nanosheets is also governed by certain factors. After manual shaking for two weeks, 40% of nanosheets prepared by the reaction with TMA^+ were thicker than 10 nm (*cf.* <2 nm for the same proportion of nanosheets prepared using TBA^+). Nanosheets became thinner with increasing the reaction time. For instance, after four weeks nanosheets prepared by the reaction with TBA^+ contained one or two layers (*cf.* two to four layers in the case of TMA^+). Exfoliation over a period of 18 weeks afforded single-layer nanosheets regardless the composition of the tetraalkylammonium (TAA^+) cation; note that diffusion of TAA^+ into the interlayer space of crystals was not the rate-determining reaction stage. The lateral size of nanosheets determined after 18 weeks reduced to 6 ± 3 μm for TMA^+ and to 4 ± 3 μm for TBA^+. This is an unavoidable feature of the preparation of single-layer nanosheets. Nevertheless, at small $TMA^+:H^+$ ratios manual shaking of TMA^+-containing dispersions for 18 weeks allows one to prepare few-layer nanosheets with a lateral size of up to 15 μm and concentration of about 4 g litre^{-1}.[84]

The higher the coverage of the surface of nanosheets in the starting crystals with hydrogen ions the easier the exfoliation. This can be illustrated taking the exfoliation of mineral birnessite (layered manganese oxide) as an example. Birnessite has the chemical composition $A_xMnO_2 \cdot y\,H_2O$, where A stands for hydrogen ions and alkali metal or calcium cations. Structurally, the compound consists of negatively charged layers containing Mn^{3+} and Mn^{4+} cations and oxygen anions; the interlayer space contains exchangeable cations and water molecules. The synthesis and exfoliation of birnessite crystals were carried out in three stages. In the first stage, hydrothermal treatment of the mixture $KMnO_4-MnCl_2-KOH$ ($Mn^{2+}:MnO_4^- = 2$ mole ratio) resulted in a soid product, potassium birnessite (from this point on, K-birnessite). According to elemental and derivatograpic analyses, the product had the chemical composition $K_{0.33}MnO_2 \cdot 0.5\,H_2O$. The unit cell constants of crystals of the product matched those of K-birnessite. Morphologically, crystals represented nanobelts several tens of micrometres long, 300–1000 nm wide and about 15 nm thick (the thickness of nanobelts was uniform throughout the length). Unbroken nanobelt ends had angular tips typical of single crystals (Fig. 4 *a*) with an angle equal to 120° (see Ref. 89). Each nanobelt was a single crystal grown along the twofold axis of the monoclinic unit cell, the wide long faces of nanobelts were indexed to {001}, while the narrow long ones were {200}. The most rapidly growing faces were {110} and $\{\bar{1}10\}$. The apex angle between them equal to 120° matched the angle at the growing nanobelt end (Fig. 4 *b*).

The authors[89] believe that growth of nanobelts is driven by hydrothermal synthesis since the reaction under non-hydrothermal conditions affords fine-crystalline powder. They pointed out that the KOH concentration (13.3 mol litre^{-1}) was the key factor of hydrothermal growth of nanobelts. This basicity of the medium allowed K-birnessite to dissolve with ease. Yet another important factor influencing the growth of nanobelts was the $Mn^{2+}:MnO_4^-$ concentration ratio. The best results were obtained at $Mn^{2+}:MnO_4^- = 2$. At $Mn^{2+}:MnO_4^- < 2$, nanobelts were shorter; at $Mn^{2+}:MnO_4^- = 1.5$, the reaction yielded micrometre-size platelets, while at $Mn^{2+}:MnO_4^- > 2$, the amount of Mn_3O_4 increased.[89]

Protonation of K-birnessite nanobelts involved two 3-h cycles of treatment of K-birnessite with 0.5 M aqueous solution of $(NH_4)_2S_2O_8$ at 60 °C and gave a product of the composition $H_{0.08}MnO_2 \cdot 0.7\,H_2O$. The proton content in this H-birnessite sample was smaller than in other samples synthesized under somewhat different conditions, namely, $H_{0.28}Na_{0.02}MnO_2 \cdot 0.8\,H_2O$,[90] $H_{0.13}MnO_2 \cdot 0.7\,H_2O$,[91] $H_{0.22}MnO_2 \cdot 0.62\,H_2O$,[92] $Na_{0.02}H_{0.34}Mn_{0.94}O_2 \cdot 0.63\,H_2O$.[93] Since $(NH_4)_2S_2O_8$ is a strong oxidizing agent, the Mn^{3+} content in

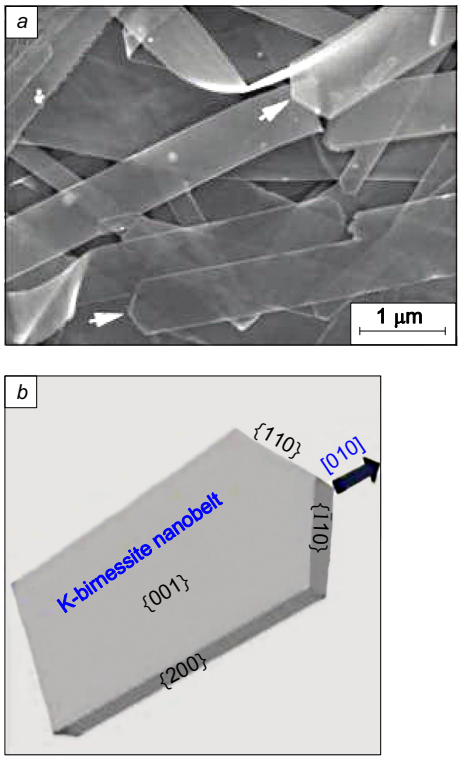


Figure 4. SEM image of birnessite nanobelts (*a*) and a birnessite crystal (*b*).[89]
White arrows are placed near angular tips.

$H_{0.08}MnO_2 \cdot 0.7\,H_2O$ was the lowest among all birnessite compositions discussed in this Section. The third stage involved exfoliation of $H_{0.08}MnO_2 \cdot 0.7\,H_2O$. Swelling of this H-birnessite in aqueous tetrabutylammonium hydroxide took 10 days at continuous shaking. Then, the dispersion was centrifuged to separate the sediment and supernatant fraction. The degree of swelling was lower than in the case of $H_{0.13}MnO_2 \cdot 0.7\,H_2O$. The supernatant dispersion contained exfoliated nanosheets with a lateral size of at most 400 nm. The exfoliation rate of H-birnessite was 25 mass % – 35 mass %.[89]

Experiments showed that the extent of osmotic swelling of $H_{0.08}MnO_2 \cdot 0.7\,H_2O$ in tetramethylammonium hydroxide solutions is much higher than in tetrabutylammonium solutions and that crystals $H_{0.28}Na_{0.02}MnO_2 \cdot 0.8\,H_2O$ and $H_{0.22}MnO_2 \cdot 0.62\,H_2O$ intercalated with tetramethylammonium ions are exfoliated upon simply washing with water due to intense osmotic swelling.[89]

A sample of $Na_{0.02}H_{0.34}Mn_{0.94}O_2 \cdot 0.63\,H_2O$ was exfoliated in aqueous tetramethylammonium hydroxide solution within 20 min under sonication. Nanosheets were separated from the dispersion medium by centrifugation and then isolated using freeze-drying process.[93]

Exfoliation of $H_{0.08}MnO_2 \cdot 0.7\,H_2O$ crystals occurred slowly[89] owing to small content of hydrogen ions and thus small amount of tetraalkylammonium ions in intercalates. Exfoliation should proceed easier in the presence of hydrophobic cations; therefore, samples swollen upon treatment with TMA^+ hydroxide and washing with water were equilibrated with TBA^+ hydroxide solutions of different concentration. Mixtures were carefully shaken and centrifuged. In the experiments with samples at $TBA^+ : TMA^+ \geqslant 100$, almost the whole amount of the solid phase precipitated upon centrifugation at 6000 rpm, whereas almost no sediment was observed at $TBA^+ : TMA^+ \leqslant 10$. X-Ray diffraction studies showed that at $TBA^+ : TMA^+ \geqslant 50$, the sediment represented swollen crystals. The interlayer distances were proportional to the square root of the molar concentration of tetrabutylammonium, thus being indicative of osmotic swelling. At $TBA^+ : TMA^+ \leqslant 25$, a halo was observed in the X-ray diffraction patterns, being indicative of the exfoliation of crystals. Lateral sizes of the exfoliated nanosheets were in the range of 300 – 1500 nm at a thickness of 0.81±0.02 nm.[89]

Not all alkali metal ions can be replaced by hydrogen ions in layered crystals. The crystal structure of layered niobate $K_4Nb_6O_{17} \cdot 3\,H_2O$ includes two alternating interlayer regions containing potassium ions (Fig. 5). Ion-exchange reactions can occur in the interlayer region I only; this was confirmed experimentally. Niobate $K_4Nb_6O_{17}$ was obtained by sintering Nb_2O_5 with K_2CO_3.[94] Subsequent refluxing of a suspension of the niobate crystals in 6 M HNO_3 for 3 days resulted in crystalline product of the composition $H_2K_2Nb_6O_{17} \cdot H_2O$. Crystals $H_2K_2Nb_6O_{17} \cdot H_2O$ and solutions R_4NOH (R = Me, Et, Pr) were stirred at room temperature for two weeks. The sediment was separated from the supernatant liquid, washed and dried. The amount of tetraalkylammonium cations intercalated into the $H_2K_2Nb_6O_{17} \cdot H_2O$ crystals was at most 50% for Me_4NOH, about 25% for Et_4NOH hydroxide and even smaller for Pr_4NOH. The content of water in the intercalated crystals decreases in the order Me > Et > Pr.

Tetrabutylammonium ions do not intercalate into the interlayer space of $H_2K_2Nb_6O_{17} \cdot H_2O$ crystals, but they facilitate exfoliation into nanosheets consisting of two layers of NbO_6 octahedra with potassium ions in the interlayer gallery. When the crystals were washed to remove the non-intercalated tetraalkylammonium hydroxide, the ionic strength of the surrounding solution decreased and a gel formed. It was assumed that the observed process represented swelling of crystals accompanied by disorganization in the arrangement of nanosheets rather than their exfoliation.

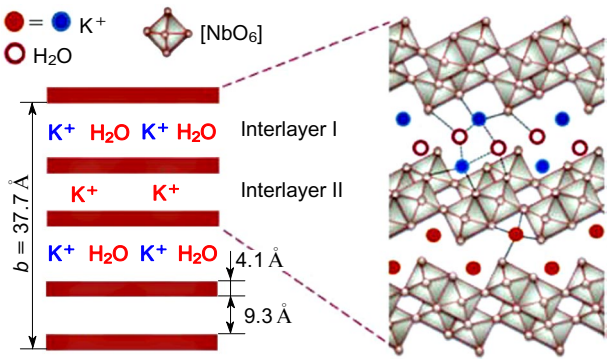


Figure 5. Crystal structure of $K_4Nb_6O_{17} \cdot 3\,H_2O$.[94]

Layered crystals can be intercalated with not only amines and tetraalkylammonium cations, but also anions. Layered double hydroxides (LDH) are related to clays and consist of positively charged brucite-like layers and hydrated anions in the interlayer space. The charge of the brucite-like layers is due to partial replacement of divalent metal ions M^{II} by trivalent metal ions M^{III}: $[M^{II}_{1-x}M^{III}_{x}(OH)_2][A^{n-}_{x/n}\cdot m\,H_2O]$, where A^{n-} stands for interlayer anions. Electrostatic attraction between layers and interlayer anions often makes exfoliation of LDH crystals difficult, in particular, in the case of crystals containing carbonate ions as interlayer anions. A carbonate Co–Al–LDH was prepared by refluxing a mixture of aqueous solutions of cobalt chloride and aluminium chloride in the presence of urea.[95] A chemical analysis of the product obtained in 97% yield gave the composition $[Co_{0.67}Al_{0.33}(OH)_2][(CO_3)_{0.165}\cdot 0.49\,H_2O]$. According to SEM data, the sample consisted of relatively thin hexagonal platelets (Fig. 6) with a lateral size of about 4 μm and a thickness of 30 nm. Sharp peaks in the X-ray diffraction pattern suggested a high quality of crystals. Replacement of carbonate ions by chloride ions occurred in a mixture of aqueous solutions of hydrochloric acid and sodium chloride. According to elemental analysis data, the product has the chemical composition $[Co_{0.66}Al_{0.34}(OH)_2][Cl_{0.34}\cdot 0.46\,H_2O]$. A SEM study showed that the size and morphology of the chloride crystals were only slightly different from those of the carbonate Co–Al–LDH.

Ion-exchange reactions between chloride and other anions were carried out by shaking mixtures of chloride Co–Al–LDH with 0.1 M solutions of corresponding acid salt. Samples of reaction products (Co–Al–LDH)X (X stands for nitrate, perchlorate, acetate, lactate, dodecyl sulfate and oleate) were isolated, dried and exfoliated by shaking mixtures containing the sample and formamide for 2 days, sediments were removed and the dispersions were centrifuged. The resulting dispersions were stable and no precipitate was observed over a long period of time, while the sediment obtained after centrifugation represented glue-like substance. The powder X-ray diffraction patterns (Fig. 7) suggested random orientation of nanosheets in the dispersion and retention of the layer structure in the crystal.

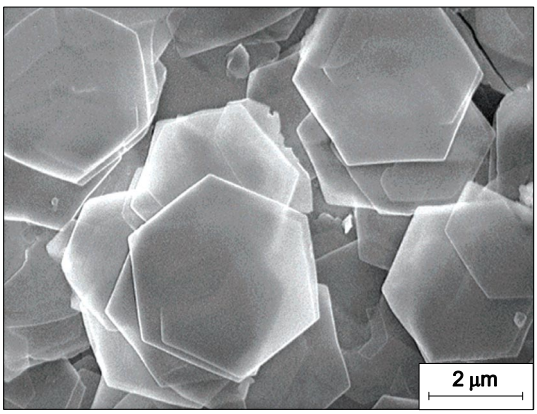
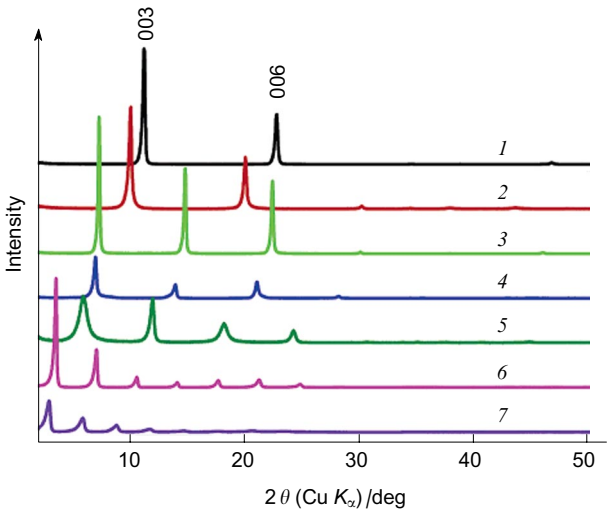


Figure 6. SEM image of Co–Al–LDH crystals.[95]



Interplanar distances

Position	1	2	3	4	5	6	7
d (003) /nm	0.78	0.89	1.19	1.27	1.49	2.51	3.02

Figure 7. Powder X-ray diffraction patterns of dispersions of (Co–Al–LDH)X systems, where X stands for chloride (*1*), nitrate (*2*), perchlorate (*3*), acetate (*4*), lactate (*5*), dodecyl sulfate (*6*) and oleate (*7*).[95]

According to AFM data, the lateral size of nanosheets was less than 2 μm, thus indicating fragmentation of nanosheets in the course of exfoliation. Nanosheets were covered with formamide molecules and the overall thickness of the LDH nanosheet and formamide molecules was 0.80 nm. Single-crystal character of the nanosheets was confirmed by selected-area electron diffraction.

This, exfoliation is a two-step process involving a fast (swelling) and a slow stage. The proportion of exfoliated crystals was 40% after 12 h and 70% after 24 h. After shaking for two days the degree of exfoliation was 75% for chloride, 50% for perchlorate, 60% for acetate and 95% for dodecyl sulfate Co–Al–LDH.

A solid solution $Li_{4x}Sn_{1-x}S_2$ corresponds to a number of stoichiometric compositions including SnS_2 ($x = 0$), $Li_2Sn_4S_9$ ($x = 0.11$), $Li_2Sn_2S_5$ ($x = 0.20$), $Li_4Sn_3S_8$ ($x = 0.25$) and Li_2SnS_3 ($x = 0.33$).[96] The crystal structure of Li_2SnS_3 ($x = 0.33$) consists of $[Li_{1/3}Sn_{2/3}S_2]^-$ layers and lithium ions in the interlayer space. All compounds and their solid solutions are prepared by sintering mixtures of lithium sulfide and elemental tin and sulfur. When in water, crystals undergo osmotic swelling and exfoliation after shaking the dispersions for 6 h. Exfoliation of $Li_2Sn_2S_5$ produces single-layer nanosheets whose lateral size (5–10 μm) and thickness (0.8–1.0 nm) match those of the starting crystals; this suggests no fragmentation of nanosheets. Exfoliation of Li_2SnS_3, $Li_4Sn_3S_8$ and $Li_2Sn_4S_9$ crystals results in few-layer nanosheets.

Dispersions are stabilized by the negative charge of nanosheets. In aqueous solutions, lithium sulfide is removed according to the equation

$$Li_{4x}[Sn_{1-x}S_2] \longrightarrow 2x\,Li_2S + [Sn_{1-x}S_{2-2x}] \quad (2)$$

and the sulfur vacancies are occupied by water molecules

$$[Sn_{1-x}S_{2-2x}] + 2x\,H_2O \longrightarrow H_{4x}[Sn_{1-x}S_{2-2x}O_{2x}] \quad (3)$$

Annealing of $H_{4x}[Sn_{1-x}S_{2-2x}O_{2x}]$ nanosheets at 450 °C is accompanied by dehydration and results in SnS_2.

It is commonly accepted that osmotic swelling is a slow process; however, time-resolved *in situ* SAXS experiments with titanate $H_{1.07}Ti_{1.73}O_4 \cdot H_2O$ revealed that the process takes a few seconds.[97] Hydroxide ions rapidly penetrated into the interlayer space of the layered crystal and reacted with hydrogen ions. Subsequent exfoliation of the crystal was followed by its immediate re-aggregation with tetrabutylammonium cations in the interlayer space. The time taken by the overall process was only slightly longer than 20 s. A 1D aggregation theory developed[98] to interpret the SAXS data was modified[99] to describe the fluctuating interlayer spacing.

Osmotic swelling of layered crystals occurs not only in water, but also in organic solvents, *e.g.*, alcohols. One-step intercalation of primary amines including n-butylamine (BA), n-hexylamine (HA), n-octylamine (OA), n-dodecylamine (DDA), n-octadecylamine (ODA) into layered titanate $K_2Ti_4O_9$ was reported.[100] Titanate powder was added to acidified aqueous amine solution at pH 7 and the mixture was stirred for 7 days. Then, the sediment was separated, washed with ethanol and dried at room temperature. Usually, amines are intercalated into layered crystals in two steps involving (i) transformation of $K_2Ti_4O_9$ into $H_2Ti_4O_9$ followed by (ii) intercalation of amines, which undergo transformation into ammonium ions in the interlayer space.[101–103]

Amine-intercalated titanates can be exfoliated in alcohols, while titanates intercalated with amines bearing long-chain alkyl substituents can be exfoliated even in nonpolar solvents, *e.g.*, toluene and hexane. The stability of dispersions was characterized by the half-life. The longest half-life equal to 96 h was found for DDA-titanate and ODA-titanate in octan-1-ol. The process results in single-layer nanosheets 1–2 nm thick (according to AFM data) with lateral dimensions up to 1–2 μm. Exfoliation with no sonication (as in the case for ODA-titanate in toluene) affords nanoribbons of length to 20 μm and width 300–500 nm (Fig. 8). Nanosheets dispersed in organic solvents coagulated in acetone. The hybrid catalyst was prepared by coating $H_2Ti_4O_9$ with 0D platinum nanocrystals.

A new exfoliation method was proposed recently.[104] Finely ground Bi_2Te_3 crystals were placed in an autoclave filled with ethylene glycol solution of lithium hydroxide (8 g litre^{-1}) and the mixture was heated at 200 °C for 24 h to achieve intercalation of lithium ions into the interlayer space of Bi_2Te_3 crystals. The sediment was filtered off, rinsed with acetone and washed with water, which led to exfoliation of crystals. The product was filtered off and dried at 60 °C or dispersed in ethanol. The authors[104] pointed out that only partial exfoliation occurred after heating for 24 h, but the process went to completion upon treatment in an autoclave for 72 h. When bulk Bi_2Te_3 crystals were used, treatment for 72 h was insufficient to complete the exfoliation.

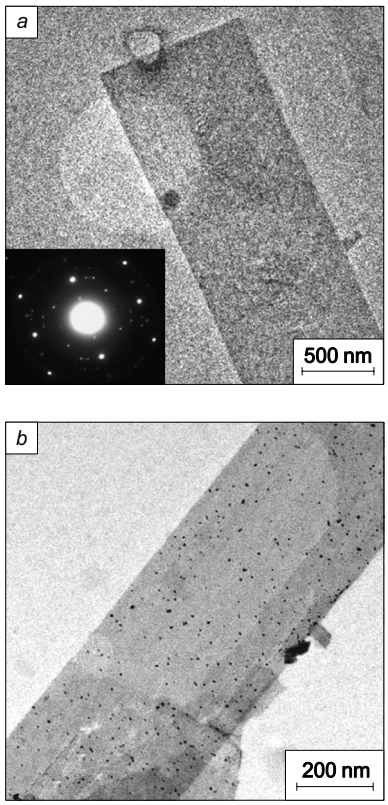


Figure 8. TEM images of $H_2Ti_4O_9$ nanobelt (*a*) (inset: SAED pattern of the nanobelt) and the same nanobelt modified with 0D platinum nanocrystals (*b*).[101]

The chemical composition and crystal structure of exfoliated nanosheets demonstrated no changes. The thickness of nanosheets determined by AFM was 3.8–3.9 nm (3–4 layers per nanosheet). The lateral dimensions of nanosheets were 200 nm for width and 1 μm for length. Assuming that ethylene glycol acts not only as solvent, but also as reducing agent, the exfoliation process was described as follows:

$$Bi_2Te_3 + y\,Li^+ + y\,e^- \longrightarrow Li_y^+(Bi_2Te_3)^{y-} \quad (4)$$

$$Li_yBi_2Te_3 + yH_2O \longrightarrow \quad (5)$$

$$\longrightarrow Bi_2Te_3(nano) + y\,LiOH + y/2\,H_2\uparrow$$

Bismuth telluride crystals do not exfoliate in aqueous lithium hydroxide solution under comparable conditions.The anion $(Bi_2Te_3)^{y-}$, which appeares in Eqn (4) and in Ref. 104, was introduced without remarks. It is strange that, although this anion displaces hydrogen from water [see Eqn (5)], hydrogen was not detected experimentally using any of the available methods. Hydrogen appears only in Eqn (5).

This approach including the concept of the exfoliation mechanism was employed by the same authors in the studies of exfoliation of Bi_2Se_3 and SnSe crystals (see Refs 105 and 106, respectively). Besides, researchers from

another group used the technique in two studies on exfoliation of SnSe under slightly different conditions:[107, 108] SnSe (1 g) was added to a solution of LiOH (0.8 g) in ethylene glycol (200 ml) and the mixture was heated in an autoclave at 473 K for 48 h. It was stated that lithium ions intercalated into the interlayer space of crystals with simultaneous reduction of SnSe with ethylene glycol to $(SnSe)^{x-}$ anion

$$SnSe + x\,Li^+ + x\,e^- \longrightarrow Li_x^+(SnSe)^{x-} \quad (6)$$

After cooling to room temperature, the sediment was filtered off, rinsed with acetone and dried *in vacuo* at 333 K for 24 h. Then the product (0.5 g) was placed in water (200 ml) and the mixture was sonicated for 1 h. It was reported that the $(SnSe)^{x-}$ anion displaced hydrogen from water. Emphasize that this research group also presented no experimental proofs of hydrogen release and no explanation for the existence of the strange anion $(SnSe)^{x-}$.

$$Li_xSnSe + x\,H_2O \longrightarrow SnSe + x\,LiOH + x/2\,H_2\uparrow \quad (7)$$

The resultant dispersion was centrifuged at 1000 rpm for 30 min, the supernatant liquid was collected and subsequently centrifuged at 8000 rpm for 30 min. The product was washed several times and dried in a vacuum oven. The lateral size of nanosheets was in the range of 200 – 500 nm and the thickness of six-layer nanosheet was 3.4 nm (AFM data). High-resolution TEM measurements confirmed single-crystal nature of the nanosheets.

Intercalation of lithium hydroxide in organic solvent followed by exfoliation is of considerable interest; however, interpretation of the mechanism of this phenomenon seems to be incorrect.

Indeed, the electrode potential of ethylene glycol is 0.0235 V *vs.* Ag – AgCl electrode[109] and therefore the standard electrode potential of ethylene glycol is nearly −0.2 V *vs.* hydrogen electrode. The standard electrode reduction potential of water

$$2\,H_2O + 2\,e^- \longrightarrow H_2 + 2\,HO^- \quad (8)$$

is −0.8277 V, *i.e.*, ethylene glycol cannot reduce water. Note that the role of anions $(Bi_2Te_3)^{y-}$ or $(SnSe)^{x-}$ and LiOH from the standpoint of electrochemistry is out of question.

It seems very likely that the authors deal with a particular case of osmotic swelling. It is an undeniable experimental fact that lithium hydroxide in ethylene glycol is intercalated into bismuth and tin chalcogenide crystals. Ethylene glycol does not follow lithium hydroxide on the way into the interlayer space. As the ethylene glycol solution of lithium hydroxide is removed and the intercalated crystals are placed in water, a high osmotic pressure is produced owing to the electrolyte (LiOH) concentration difference between the interior of the crystals and the external medium. This gives rise to osmotic swelling resulting in exfoliation of crystals. Emphasize the high value of this method of exfoliation because it extends the range of crystals that can be exfoliated using osmotic swelling in organic solvents.

5. Chemical and electrochemical intercalation

Intercalation of lithium into MoS_2 crystals has long been known.[1] Typically, a MoS_2 powder is mixed with hexane solution of n-butyllithium and the mixture is allowed to stand in nitrogen atmosphere for 48 h. At room temperature, n-butyllithium decomposes into lithium atoms and octane; lithium atoms incorporate into the interlayer space of MoS_2. Intercalated MoS_2 crystals are treated with water. Hydrogen evolved pushes MoS_2 layers apart from one another to give a dispersion of MoS_2 nanosheets in water. Lithium hydroxide is removed from chemically exfoliated MoS_2 in water stream for 7 days. The lateral size of nanosheets (0.7 μm) and their thickness (~0.8 nm for single-layer and 1.5 nm for bilayer nanosheets) were determined by AFM.[110]

Selected-area electron diffraction patterns revealed the presence of two crystalline polymorphs, 2H-MoS_2 and 1T-MoS_2. This means that exfoliation of lithium-intercalated MoS_2 crystals produces nanosheets belonging to two phases with different coordination environment of molybdenum atoms surrounded by sulfur atoms, namely, trigonal prismatic (2H) and octahedral (1T). The 1T crystalline phase is metastable and exhibits metallic conductivity, whereas the 2H phase has the properties of a semiconductor. It was found that the structure of a MoS_2 nanosheet produced by exfoliation of lithium-intercalated crystals consists of nanometre-size domains of both phases, being strongly distorted in certain regions due to clusterization of molybdenum atoms.[111, 112] The structures of some nanosheets demonstrate holes.

An electrochemical method of controllable lithium intercalation into layered transition-metal dichalcogenide crystals by controlling the discharge processes was developed.[113] The layered crystal was incorporated into the electrochemical cell as cathode, while lithium foil served as anode (Fig. 9). Intercalation was conducted in $LiPF_6$ at room temperature over a period of 6 h. As the process completed, the residual electrolyte was removed with acetone and the intercalated crystals were exfoliated under sonication in water or ethanol. This was accompanied by the evolution of hydrogen or ethane, respectively, which delaminated the crystal along with cavitation bubbles. The dispersion thus prepared was centrifuged, washed with water six times and then redispersed in water. It was found that the yield of nanosheets depends on the effective area of the electrode,[113] but the yield value was not specified. Mention was only made of

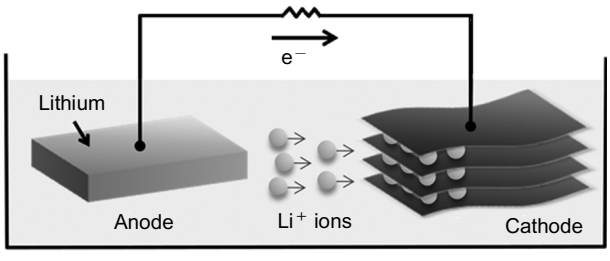


Figure 9. Electrochemically controlled lithiation of transition metal dichalcogenides: a schematic.[113]

2 mg of nanosheets prepared (the mass of the starting material is also unknown) and paste of the transition-metal dichalcogenide crystals stuck to the electrode. According to AFM data, 92% of the nanosheets were single-layer and had a thickness of about 1 nm.

The structure of the Li_xMoS_2 intercalates depends on the content of lithium. At $x = 1.3$, the 2H to 1T phase transition is completed. The formation of metallic molybdenum and lithium sulfide was observed at $x = 3$.

This approach was employed for exfoliation of WS_2, TiS_2, TaS_2 and ZrS_2 crystals. The nanosheets thus produced were used to fabricate field-effect transistors and nitrogen oxide sensors. It was reported that lithium-intercalated TaS_2 can be exfoliated in water with ease, after short-term manual shaking of the dispersion.[114] Layered crystals can be intercalated with not only lithium, but also sodium or potassium atoms.[115]

Electrochemical methods also enable intercalation of transition-metal dichalcogenides with anions that undergo transformation into gases upon oxidation in the interlayer space. For instance,[116] a bulk MoS_2 crystal, a platinum wire and a 0.5 M Na_2SO_4 solution were used as the working electrode, counterelectrode and electrolyte, respectively. The electrodes were connected to a d.c. power supply. Initially, a bias of +2 V was applied for 10 min to wet the bulk MoS_2 crystal. Then, the bias was increased to +10 V for 0.5–2 h to exfoliate the MoS_2 crystal. The exfoliated nanoflakes were collected using vacuum filtration and dispersed in *N*-methylpyrrolidone. The concentration of colloidlal solution was in the range of 0.007–0.014 g litre^{-1}. The yield of exfoliation was 5%–9%.

It is believed[116] that positive potential of the working electrode causes the oxidation of water and formation of $^{\bullet}OH$ and $^{\bullet}O^{\bullet}$ radicals, which insert themselves and/or SO_4^{2-} anions between the MoS_2 layers, thus weakening the interlayer van der Waals interactions. Further oxidation of the sulfate anions leads to formation of gaseous oxygen and hydrogen sulfide, the MoS_2 interlayer distances hugely expand, the bulk crystal exfoliates and the MoS_2 nanosheets form a dispersion in the aqueous electrolyte solution. Of course, the MoS_2 nanosheets thus prepared have partially oxidized surface, but a proper choice of exfoliation conditions minimizes the extent of oxidation.

The lateral size of the electrochemically exfoliated nanosheets reached a value of 50 μm. It was determined that the nanosheets had different number of layers. This was explained by nonuniform distribution of surface resistance over the contact area on the working electrode.

Electrochemical exfoliation can be achieved without preliminary intercalation of layered crystals. For instance, black phosphorus is a direct gap semiconductor with layered crystal structure. Its bandgap depends on the number of layers per nanosheet.[19] Electrochemical exfoliation of black phosphorus crystals was carried out[117] in such a manner that the crystals, a platinum foil and a 0.5 M sulfuric acid solution were used as anode, cathode and working electrolyte, respectively. Applying a voltage of +3 V caused exfoliation of the crystals and the solution turned orange. After 2 h, a sediment that formed at the bottom of the electrochemical cell was washed with water, filtered off, dried and dispersed in DMF under sonication for 1 h. The lateral size of nanosheets was 1×2 μm^2. The thickness of nanosheets was not measured, only the electron microscope image contrast was compared.

6. Exfoliation by hydrazine

Exfoliation of MoS_2 crystals using four hydrazine derivatives including hydrazine hydrochloride, 1,2-dimethylhydrazine hydrochloride, *tert*-butylhydrazine hydrochloride and phenylhydrazine hydrochloride was reported.[118] The authors of that study believed that bulky molecules of the four compounds presented great steric hindrance to intercalation into the interlayer space of MoS_2 crystals and proposed their own method. For each hydrazine derivative, a 10 ml portion of 0.05 M solution in DMF was brought to reflux and 2 g of bulk MoS_2 powder was added upon reaching reflux. The reaction mixtures were refluxed for 1 h, cooled in a cold water bath and centrifuged at 200 g for 90 min to remove the unreacted MoS_2 powder. The supernatant liquids were centrifuged at 19 000 g to isolate the MoS_2 nanosheets. Then, the sediments were collected, washed with water three times to remove water-soluble impurities, resuspended in DMF and centrifuged at 19 000 g three times to remove water. Exfoliation as a result of the interaction of hydrazine with MoS_2 was accompanied by reduction of the nanosheets to the chemical composition $MoS_{1.2}$, as was detected by X-ray photoelectron spectroscopy (XPS). The band gap of $MoS_{1.2}$ determined from the XPS spectra was 2.1 eV, being significantly different from that of MoS_2 (1.85 eV).

The lateral size of nanosheets ($\sim$1 μm) was approximately half the size of the precursor crystal. The nanosheets were amorphous, which is not surprising if we take account of strong compositional changes. Since experiments with all the four hydrazine derivatives led to identical results, it was concluded that hydrazine does not penetrate into the interlayer space of MoS_2 crystals and that the crystals experience layer-by-layer exfoliation owing to a reduction reaction responsible for the changes in the chemical composition and size of the nanosheets. The thickness of the nanosheets determined by AFM was 1.9 ± 0.2 nm, which corresponded to two $MoS_{1.2}$ layers, and the nanosheet thickness distribution was very narrow.

A vivid example is provided by exfoliation of bismuth sulfide.[119] Structurally, Bi_2S_3 consists of nanoribbons held together by van der Waals forces. Since exfoliation of Bi_2S_3 crystals can result in the formation of 1D nanowires, the process was tuned to produce nanosheets instead of nanoribbons. A mixture of hydrazine dihydrochloride (0.5 g) and Bi_2S_3 (0.1 g) in DMF (10 ml) was heated to reflux at 153 °C for 1 h with continuous stirring. The remaining organic side products were solidified at −30 °C for 1.5 h and all solid phases including the unexfoliated Bi_2S_3 were removed after centrifugation at 200 g for 15 min. The dispersion thus obtained was centrifuged at 16 000 g for 1 h. As a result, the sediment representing ultrathin nanosheets was collected, washed with DMF and then dispersed in fresh portion of DMF for further analysis. The yield of exfoliation[119] was high, although no numerical data were reported.

Since Bi_2S_3 interacts with hydrazine in the course of exfoliation, its chemical composition changes to $Bi_2S_{2.6}$,

as was proved by XPS. Compound $Bi_2S_{2.6}$ is a p-type semiconductor. Its nanosheets appeared to be promising for application as nitrogen dioxide sensors. The lateral size of $Bi_2S_{2.6}$ nanosheets was mainly in the range of 3 – 7 μm (maximum lateral size was 17 ± 1 μm). Probably, the size of the nanosheets was specified by the size of the starting crystals. The thickness of $Bi_2S_{2.6}$ nanosheets was determined by AFM and that of corroborated samples was measured by TEM. The minimum thickness of the nanosheets was 1.5 nm, the nanosheet thickness distribution had a maximum at 2.5 nm and slowly faded out in the interval 3 – 5.5 nm.

Two-step intercalation of TMD by hydrazine allows one to prepare nanosheets with unprecedentedly large surface area.[120] In the first stage MoS_2 crystals were intercalated with hydrazine hydrate in autoclave at 130 °C for 48 h. As result, a 100-fold expansion of the crystals occurred due to the formation of gaseous species. These crystals were washed with water three times and dried at 120 °C for 10 h. In the second stage, the expanded MoS_2 crystals were intercalated with alkali metal atoms by mixing with lithium, sodium or potassium naphthalenide solutions in anhydrous tetrahydrofuran for 5 h. Solid residues were rinsed with tetrahydrofuran. Finally, the alkali-metal intercalated crystals were exfoliated in water under sonication. The dispersion thus formed was centrifuged to separate the unexfoliated MoS_2 crystals. The supernatant liquid was re-centrifuged to isolate the nanosheets. Most nanosheets (80%) had a lateral size of at least 10 μm and a surface area of ~400 μm^2. The nanosheet thickness determined by AFM was typically 1 nm, which corresponded to single atomic layer. A statistical analysis showed that 80, 90 and 20 out of 100 Li_xMoS_2, Na_xMoS_2 and K_xMoS_2 nanosheets, respectively, were one layer thick.

Two-step exfoliation of TiS_2, TaS_2 and NbS_2 crystals produced single-layer nanosheets while that of $TiSe_2$, $NbSe_2$ and $MoSe_2$ crystals afforded two- to four-layer ones.

These experimental facts were interpreted as follows: the first step of intercalation involves partial oxidation of hydrazine to $N_2H_5^+$. Hydrazinium cation is thermally unstable and decomposes in autoclave into N_2, NH_3 and H_2. Intercalation with alkali metals and subsequent treatment of intercalates with water complete the exfoliation of MoS_2 crystals. Organic naphthalenide anion is not intercalated into MoS_2.

This interpretation seems to be contradictory. First, the (002) interlayer distances in the intercalates Li_xMoS_2, Na_xMoS_2 and K_xMoS_2 demonstrate a respective increase by 2.1%, 16.7% and 31.1% compared to those in the untreated MoS_2. This is much smaller that the 100-fold expansion achieved after swelling in the first step of the process and means a dramatic reduction of the volume of the hydrazine-treated crystal upon the intercalation of alkali metals. Methods used to evaluate the degree of expansion of the crystal volume ('100-fold increase') after intercalation of hydrazine were not specified. The possibility of one-step preparation of nanosheets by intercalation of hydrazine (no intercalation of alkali metals) was not discussed.

Next, it was stated that, according to XPS data, nanosheets exfoliated using sodium naphthalenide have the structure of the 2H-polymorph. However, this phase demonstrated no photoluminescence. Indeed, photoluminescence was observed only after heating of exfoliated MoS_2 to 200 °C, so one can assume that the nanosheets had the structure of metastable 1T-polymorph and then were transformed to the 2H-polymorph by heating.

Third, it was reported that Li_xMoS_2 crystals warmed-up on contact with air, Na_xMoS_2 crystals spontaneously ignited, while K_xMoS_2 crystals spontaneously exploded. It was also reported that storage in moist atmosphere for three days caused the (002) interlayer distances in all the three compounds to increase due to intercalation of atmospheric water with the formation of $Li_x(H_2O)_yMoS_2$, $Na_x(H_2O)_yMoS_2$ and $K_x(H_2O)_yMoS_2$ without self-explosion or self-ignition. Being undoubtedly of considerable interest, the two-step exfoliation technique requires clarification.

7. Exfoliation by ionic liquids

Ionic liquids (ILs) are rarely used for exfoliation of crystals, probably, since they are expensive. However, the available experimental data and results of calculations demonstrate that ILs are suitable for exfoliation.

Four ILs, *viz.*, 1,2-dimethyl-3-R-imidazolium tetrafluoroborates [R = propyl ($MMPI^+$), butyl ($MMBI^+$), decyl ($MMDI^+$) and hexadecyl ($MMHdI^+$)], were tested in the experiments on exfoliation of layered dichalcogenide TiS_2.[121] Three different methods of intercalation using ILs included electrochemical intercalation and two liquid-phase techniques (in acetonitrile solutions of ILs and in pure ILs on heating). Among them, the most efficient is the intercalation of mixtures of TiS_2 with $MMPIBF_4$, $MMDIBF_4$ and $MMHdIBF_4$ in pure ILs on heating at 60, 150 and 150 °C, respectively, over a period of seven days. The main goal of these experiments was to determine whether ILs can intercalate into TiS_2 by analogy with surfactants. High polarity of ILs suggested the feasibility of intercalation.

All pure ILs were found to intercalate into TiS_2 on heating.[121] According to powder X-ray diffraction data, alkyl-substituted imidazolium rings are arranged perpendicular to the TiS_2 layers in the interlayer space. Cations $MMHdI^+$ form double layers where the cations face each other by the alkyl substituents, while the imidazolium rings face the TiS_2 layers (Fig. 10 *a*). This arrangement of the $MMHdI^+$ cations leads to expansion of the distances between TiS_2 layers from 5.57 Å in the untreated TiS_2 to 54.36 Å in the intercalated compound.

Cations $MMDI^+$ form double layers with alternating head-to-tail orientations of imidazolium rings (Fig. 10 *b*).

Intercalation of pure $MMPIBF_4$ (no solvent) led to formation of two phases with different arrangement of the $MMPI^+$ cations relative to TiS_2 sheets. Namely, the imidazolium ring planes are perpendicular to the TiS_2 sheets in one phase (Fig. 10 *c*) and tilted relative to the TiS_2 sheets in the other phase (Fig. 10 *d*). Electrochemical intercalation of $MMPIBF_4$ in acetonitrile solution produces a two-phase mixture of the starting TiS_2 with the insertion phase of $MMPIBF_4$ into the interlayer space of TiS_2; here, the imidazolium ring planes of $MMPIBF_4$ are arranged parallel to the TiS_2 sheets (Fig. 10 *e*).

The possibility of exfoliation of hexagonal boron nitride (h-BN) using ILs has been discussed.[122] The free energies of solvation of h-BN nanosheets in the course of

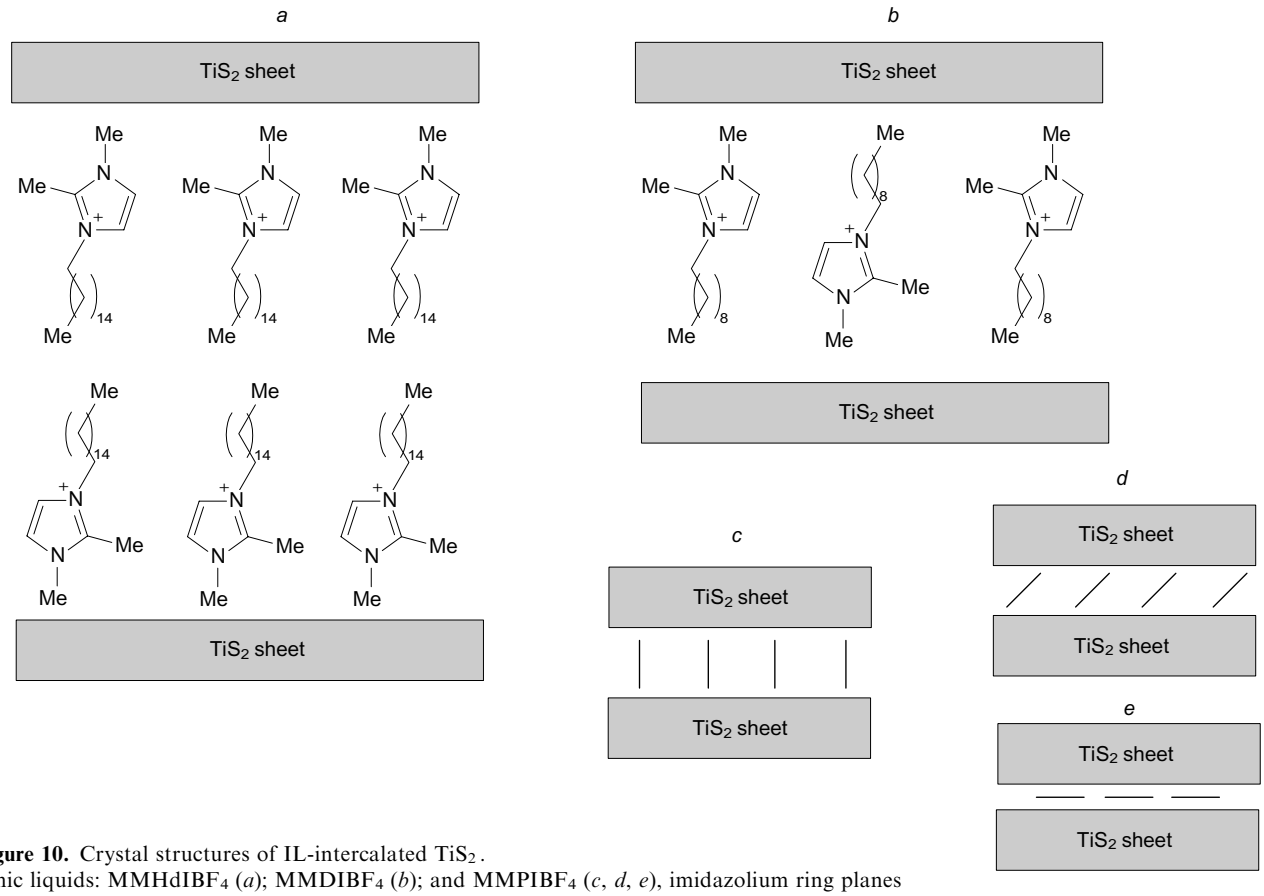


Figure 10. Crystal structures of IL-intercalated TiS_2.
Ionic liquids: $MMHdIBF_4$ (*a*); $MMDIBF_4$ (*b*); and $MMPIBF_4$ (*c*, *d*, *e*), imidazolium ring planes are perpendicular to, tilted relative to or parallel to planes of TiS_2 sheets, respectively.

exfoliation of h-BN double layers in the presence of three ILs containing different cations and same-type anion were calculated.[123] The model cations were 1-butyl-3-methylimidazolium $[bmim]^+$, 1-methylpyridinium $[C_4Py]^+$ and *N*-butyl-*N*-methylpyrrolidonium $[Pyrr_{14}]^+$, while the model anion was bis(trifluoromethylsulfonyl)-imide NTf_2^-.

The preferability of these ILs for exfoliation of h-BN decreases in the order $[C_4Py]^+ > [Pyrr_{14}]^+ > [bmim]^+$ following the decrease (in magnitude) of the calculated free energies of exfoliation equal to −970, −849 and −832 kJ mol^{-1}, respectively. These values are roughly similar to a value of −908.54 kJ mol^{-1}, *i.e.*, the calculated free energy of *N*-methyl-2-pyrrolidone (MNP) that was used earlier for exfoliation of h-BN.

Yet another argument for the use of ILs to exfoliate h-BN is related to the surface tension. Experience showed that solvents whose surface tension is close to that of powder-like h-BN (47–63 mJ m^{-2}) are suitable for exfoliation of h-BN. The surface tension of various ILs is in the range of 33–45 mJ m^{-2}; therefore, one can expect that ILs can be utilized for liquid-phase exfoliation of h-BN.

When analyzing the results of calculations, certain atom–atom interactions between ILs and h-BN deserve attention. The IL cations mainly interact with nitrogen atoms of h-BN. In $[bmim]^+$, butyl carbon atoms interact with h-BN nanosheets stronger than the ring or methyl carbon atoms. This resembles the interaction of $[bmim]^+$ with graphene[124] where π–π-interaction between the imidazolium ring and the basal plane of the graphene sheets is not the major stabilizing interaction, as was assumed earlier.[125] The results of calculations suggest the presence of long-range electrostatic interactions and, possibly, anion–π-electron interactions between NTf_2^- anion and the h-BN nanosheet; the latter were not predicted by the calculations for graphene. Weak hydrogen bonds exist between the C(2) proton of $[bmim]^+$ and the nitrogen atoms of h-BN.

The interaction between IL $[Pyrr_{14}][NTf_2]$ and h-BN mainly occurs through butyl and methyl carbon atoms, whereas h-BN does not interact with atoms of the pyrrolidinium ring. Eventually, $[C_4Py][NTf_2]$ more likely interacts with h-BN through butyl groups rather than π–π-interaction between pyridinium and h-BN. This differs h-BN from graphene for which π–π-interaction with pyridinium was found to dominate.

Concluding this Section, we will dwell on yet another example. A 0.05% dispersion of hexagonal plate-like Bi_2Te_3 crystals 1–2 μm wide and ~50 nm thick in 1-n-butyl-3-methylimidazolium chloride (IL $[C_4mim]Cl$) was tip sonicated at 80–150 °C for 1 h to exfoliate the crystals.[126] According to AFM data, the nanosheets thus prepared were 15 ± 8 nm thick. The dispersion was stable over a period of 30 days. A molecular dynamics simulation of the mechanism of exfoliation showed that nanosheets covered with telluride ions undergo a parallel shift towards one another and are immediately solvated by the

IL owing to the interaction between the negatively charged telluride ions and imidazolium cations. The latter form a dense layer on the nanosheet surface while chloride anions are in the diffuse layer of the electrical double layer that stabilizes the dispersion.

A molecular dynamics study of the interaction of eight ILs of the compositions C_4mimA and C_2mimA (A = NTf_2^-, PF_6^-, Br^-, Cl^-) with Bi_2Te_3 crystals is available.[127] Three exfoliation mechanisms considered were pulling, shearing and peeling.

The peeling mechanism was found to be most efficient since the exposed surface is gradually covered with the IL (although the shearing-driven process seems to proceed identically). Among the eight anions studied, NTf_2^- appeared to be most preferable for exfoliation.

8. Exfoliation in supercritical fluids

Supercritical carbon dioxide ($scCO_2$) is a promising agent for exfoliation of layered materials. Owing to low viscosity it penetrates into layered structures and expands after rapid depressurization, thus breaking up the interlayer bonds. Various additives dissolved in $scCO_2$ diffuse into the interlayer space of crystals along with carbon dioxide and cover the surface of nanosheets after depressurization and evaporation of solvent, thus precluding aggregation of the nanosheets.[128]

Two-dimensional crystals of BN, MoS_2 and WS_2 were exfoliated in $scCO_2$ under sonication without using stabilizers to preclude self-assembly of the layers. The exfoliation products were washed with anhydrous ethanol. Solutions of the exfoliated materials in ethanol were stable over a period of a few hours depending on the concentration of the nanosheets. According to AFM data, the thickness of nanosheets was 0.5 nm for BN and 0.75 to 0.80 nm for MoS_2 and WS_2; the lateral size was 0.5 – 2 μm. Among the BN nanosheets, 90% were less than five layers thick, 40% were two layers thick and 20% were single-layer.[129]

Exfoliation of a titanate material in supercritical DMF produced TiO_2 nanosheets.[130] Flux-grown $K_{0.8}Ti_{1.73}Li_{0.27}O_4$ crystals were transferred to hydrochloric acid solution and the solution was stirred for five days to obtain $H_{1.07}Ti_{1.73}O_4 \cdot H_2O$ crystals, which were filtered off and dried. Then the sample (20 mg) was mixed in DMF (10 ml) and exfoliation was carried in a closed steel vessel under sonication for 15 min. Following exfoliation, the reactor was heated to 400 °C (*cf.* 377°C for the critical temperature and 4.4 MPa for the critical pressure of DMF). The exfoliated nanosheets were fragmented (Fig. 11). The lateral dimensions of many fragments were larger than 5 μm, while the thickness was 1.2 – 1.5 nm (AFM data). High-resolution TEM and SAED measurements confirmed the single-crystal nature of the nanosheets that were specified as titania; however, no experimental proofs were presented. It seems likely that heating in DMF to 400 °C was a satisfactory argument supporting dehydration of the starting $H_{1.07}Ti_{1.73}O_4 \cdot H_2O$ and formation of TiO_2.

Layered titanate $K_{0.8}[Ti_{1.73}Li_{0.27}]O_4$ was treated with HCl to prepare the protonated form $H_{1.07}Ti_{1.73}O_4 \cdot H_2O$, which was heated in supercritical DMF or in supercritical water over different periods of time (from 15 min to 10 h) to study the phase transition of the material.[131]

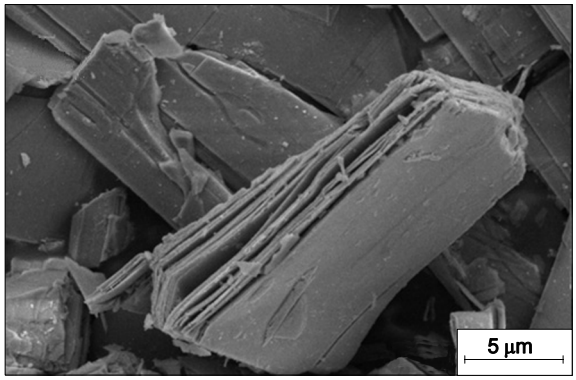


Figure 11. SEM image of $H_{1.07}Ti_{1.73}O_4 \cdot H_2O$ crystals exfoliated in supercritical DMF.[130]

Exfoliation did occur in supercritical DMF, while in supercritical water at 400 °C the layered protonated titanate transformed into anatase without exfoliation. At lower temperatures, water did not reach the supercritical state.

9. Separation and size control of nanosheets

Liquid-phase exfoliation produces nanosheets with broad lateral size (L) and thickness (N) distributions (here, the thickness is expressed as the number of layers per nanosheet). Optoelectronics uses nanosheets of specified thickness,[36] while many other applications require nanosheets of specified size. The development of methods for fractionation of dispersions has become topical. The proportion of single-layer nanosheets is always small

Thickness sorting and lateral size separation of 2D nanocrystals require continuous control of the particle size using methods suitable for large-scale applications, namely, methods for the determination of the size of nanosheets in flow systems.

Dispersions of MX_2 nanosheets (M = Mo, W; X = S, Se) can be fractionated into fractions corresponding to particular numbers of single layers per nanosheet using a method called isopycnic 'density gradient ultracentrifugation' (DGU). Nanosheets are separated in a dispersion medium representing an aqueous solution of a substance whose density is higher than that of water. The dispersed phase contains nanosheets prepared from molybdenum disulfide or its analogues (see above) and surfactant molecules that cover the surface of the nanosheets. The technique involves creation of a density gradient in the dispersion medium during centrifugation. At centrifugal accelerations of a few thousand g, the more dense cosolvent moves towards the bottom of the ultracentrifuge tube, while water is displaced towards the top. As a result, the dispersed phase is separated into layers (bands) of different density, arranged perpendicular to the tube axis. Molybdenum sulfide nanosheets are in the layer whose density matches that of a surfactant-covered nanosheet since the nanosheet goes down in the less dense layers and comes to top in the more dense ones. Thickness sorting of nanosheets is performed using layer-

by-layer selection of the dispersion formed after centrifugation.[132]

This general scheme has a number of distinctive features. Molybdenum sulfide crystals are exfoliated under sonication in 20% aqueous solution of $HO[(CH_2)_2O]_n[CHMeCH_2O]_m[(CH_2)_2O]_nH$ nonionogenic surfactant (Pluronic F68), which is necessary to prevent aggregation of exfoliated crystals. The degree of exfoliation is less than 100%; the dispersion is collected to dispose of unexfoliated crystals. To this end, 32 ml of dispersion prepared after sonication-assisted exfoliation was added on top of a 6 m underlayer of 60% iodixanol solution (density 1.32 g ml^{-1}) containing 2% F68. The mixture was centrifuged at 32 000 rpm at room temperature for 24 h. Then, 5 ml of 60% iodixanol solution containing 2% F68 was injected above the sediments at the bottom of the ultracentrifuge tube to separate the dispersion. The dispersion thus prepared was stable over a period of a few months. Preliminary experiments showed that yet another surfactant, sodium cholate, is inefficient in exfoliation of MoS_2.[132]

The dispersion was subjected to two-step separation using DGU. First, the dispersion was placed at the bottom of an iodixanol layer and the mixture was ultracentrifuged at 28 000 rpm for 12 h. As a result, the dispersion became separated into visible bands throughout the ultracentrifuge tube. All coloured bands were recovered and the separation procedure was repeated. The yield of single-layer nanosheets was very low, *viz.*, treatment of 1 g of bulk MoS_2 crystals gave 0.0065 mg of single-layer MoS_2 nanosheets.[132]

Density gradient ultracentrifugation was also used for separation of graphene nanosheets.[133]

Size-selected dispersions of MoS_2 nanosheets can be obtained by fractionation of the dispersed phase using cascade centrifugation. This technique is based on the difference between the nanosheet deposition rates. A layer of stock dispersion prepared upon exfoliation was added on top of a higher-density liquid filling the centrifuge tube and centrifuged without mixing at moderate speed for 10–40 min. The largest nanosheets moved down while the smallest ones remained at the top of the centrifuge tube. The dispersion was separated into seven fractions throughout the tube, each fraction was recovered and analyzed. The extinction spectra (Ext) of these fractions were measured. Extinction, or the sum of scattering and absorbance contributions, is also related to optical transmittance (Tr) as follows:

$$\mathrm{Tr} = 10^{-\mathrm{Ext}} \qquad (9)$$

The extinction spectra of all fractions were different from one another, the differences originating from the size of nanosheets. The sum of the extinction spectra of all fractions matched the extinction spectrum of the starting dispersion prepared upon liquid-phase exfoliation.

The extinction spectra of all fractions were normalized to the absorbance at 345 nm, and all the extinction spectra exhibited the *A*- and *B*-exciton peaks (Fig. 12). The *B*-exciton peak at 605 nm was used for quantitative characterization of the differences between the extinction spectra of all fractions using the $\mathrm{Ext}_B/\mathrm{Ext}_{345}$ ratio that increased fourfold from fraction 1 to fraction 7. Since no

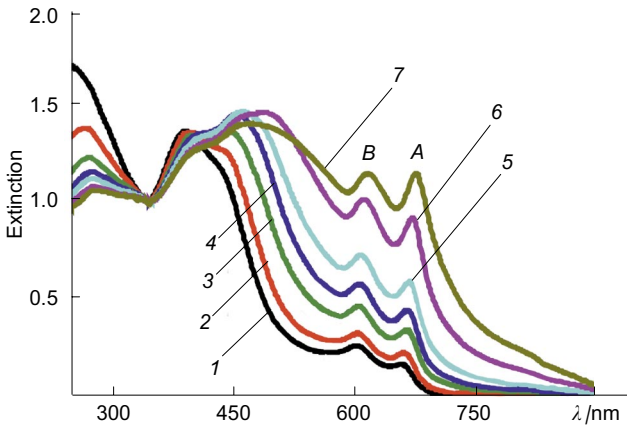


Figure 12. Extinction spectra of the MoS_2 fractions normalized to the local minimum at 345 nm.[134]
A and *B* denote the positions of the *A*- and *B*-excitons; the numbers *1*–*7* denote the fractions of the dispersion. The thickness and lateral size of nanosheets increase with the fraction number.

such matter was observed in the extinction spectra of films of re-stacked chemically exfoliated nanosheets of different thickness, it was assumed that the spectral differences between fractions are related to changes in the lateral size of the nanosheets. The larger the amount of individual nanosheets and the smaller the amount of stacked nanosheets the larger the total edge length of the nanosheets and the greater the edge-effect-driven impact on the extinction spectra.[134]

It was also found that the position of the *A*-exciton on the wavelength scale in the extinction spectra undergoes a bathochromic (red) shift as the fraction number (*i*.e., the number of layers per nanosheet) increases due to the confinement effect and can be used to determine the thickness of nanosheets.[134]

A fundamental difference between the extinction spectra of dispersions and true solutions consists in that the spectra of the latter include no contribution from the scattering coefficient, so the extinction spectra match the absorbance spectra. The extinction spectra of dispersions represent superpositions of the absorbance spectra and scattering coefficient spectra. The contribution of scattering is especially great for nanosheets with large lateral size. To take into account the effects of scattering on the absorbance spectra, a number of size-selected dispersions were prepared. Their concentrations were found by filtering the dispersed phase and weighing to determine the extinction, absorption and scattering coefficients. The extinction spectra were converted to the extinction coefficient spectra $\mathrm{Ext} = \varepsilon Cl$, where ε is the extinction coefficient, C is the dispersion concentration and l is the cell length of the spectrometer. The integrating sphere of the spectrometer was used to separate the contributions of absorbance and scattering. This made it possible to plot the absorption (α) and scattering (σ) coefficient spectra. By definition,[134] at the wavelength λ one has

$$\varepsilon(\lambda) = \alpha(\lambda) + \sigma(\lambda) \qquad (10)$$

The extinction spectra contain information on the length of nanosheets. To extract these data, a number of fractions of the starting dispersion were studied by TEM. A statistical analysis of the length of nanosheets isolated from the size-selected dispersions prepared by cascade centrifugation and from dispersions prepared by centrifugation at different rotation speed showed that the former are characterized by narrower nanosheet size distributions. It was found that at $\lambda = 345$ nm, ε is almost invariant with respect to the fraction number and, therefore, the lateral size of the nanosheet. This allows one to determine the concentration of dispersions containing nanosheets of any size from the extinction spectra (this holds at $L < 300$ nm).[134]

The lateral size of nanosheets is related to the $\mathrm{Ext}_B/\mathrm{Ext}_{345}$ ratio (Ext_B and Ext_{345} are the extinctions at the *B*-exciton wavelength and at 345 nm, respectively). It was assumed that this is due to the impact of the edge effects on the local electronic structure, the density of states and, therefore, the local optical absorption coefficient of the nanosheets. The observed absorption spectrum is the sum of the edge and centre contributions.[135]

Since the ratio of the edge length to the surface area increases as the size of nanosheets decreases, one can expect that the spectral pattern will be nanoparticle size dependent. Nanosheets of arbitrary shape can be approximated using two parameters, the length L and the aspect ratio $k = L/x$ (x is the width of the nanosheet). Then one has[134]

$$\alpha \approx \alpha_C \left[1 + \frac{2x}{L}(k+1)\frac{\Delta\alpha}{\alpha_C}\right] \tag{11}$$

Here $\Delta\alpha = \alpha_E - \alpha_C$, α_E and α_C are the absorption coefficients of the nanosheet edges (E) and centre (C), respectively. Equation (11) reasonably described experimental data at $L > 60$ nm. Calculations for smaller nanosheets were complicated by the errors due to the edge effects.[134]

Electron energy loss spectroscopy (EELS) and XPS studies showed that the electronic structures of the near-edge and central regions differ significantly and that the width of the edge region is variable.

The length of nanosheets was determined using the empirical relationship which takes account of the edge effect,[134]

$$L = \frac{3.5\mathrm{Ext}_B/\mathrm{Ext}_{345} - 0.14}{11.5 - \mathrm{Ext}_B/\mathrm{Ext}_{345}} \tag{12}$$

where the nanosheet length L is given in micrometres. The error in the determination of L values was estimated at $<10\%$. This allowed one to evaluate the length of nanoflakes in fractionated dispersions containing nanosheets of any length in the range between 70 and 350 nm by measuring the extinction spectra. Estimates for larger nanosheets ($L > 350$ nm) can be obtained using specific methods of calculation.

To understand the text below, mention should be made of the following. In contrast to multilayer MoS_2 crystals, single-layer MoS_2 nanosheets are direct gap semiconductors and their fluorescence spectrum exhibits a narrow peak at $\lambda_{\mathrm{emission}} = 651$ nm (full width at half-maximum is 23 nm). The fluorescence spectrum ($\lambda_{\mathrm{exc}} = 435$ nm) is size independent and, therefore, shows no pronounced edge effect except a decrease in the fluorescence intensity from very small nanosheets. Fluorescence from bilayer nanosheets is characterized by much lower quantum efficiency.

The thickness of nanosheets was determined using the confinement effect. Relevant experimental information was extracted from the position of the *A*-exciton peak in the extinction spectra. First of all, a method was elaborated for experimental determination of the thickness of nanosheets using AFM and combination of fluorescence spectra and Raman scattering (single-layer MoS_2 nanosheets luminesce, but the glow rapidly weakens with increasing the number of layers in the nanosheets). This made it possible to evaluate the averaged thickness of nanosheets expressed as the number, N, of layers per nanosheet and to relate it to the *A*-exciton wavelength. The empirical equation is valid for MoS_2 only and has the form[134]

$$N = 2.3 \times 10^{36} \mathrm{e}^{-54.888/\lambda_A} \tag{13}$$

where λ_A is the *A*-exciton wavelength. Thus, the averaged number of layers can be assessed from the extinction spectra. Emphasize that expressions (12) and (13) are independent.

At $N \geqslant 10$, the extinction and absorbance diverge because of increasing contribution of scattering. Therefore, formula (13) holds only at $N < 10$. Meanwhile, it is unnecessary to measure nanosheets with $N \geqslant 10$ since their properties do nor differ from those of bulk crystals.[134]

Tungsten disulfide has much in common with MoS_2, but the spectral bands of single-layer WS_2 nanosheets are shifted towards the long-wavelength (red) region and are stronger than the bands of the central regions of the nanosheets. It follows that the band gap in the near-edge region is narrower than in the central regions of nanosheets. This is consistent with the results published earlier.[136]

Liquid-phase cascade centrifugation for size selection of nanosheets was developed in reference to tungsten disulfide. A dispersion prepared by sonication-assisted exfoliation of WS_2 in aqueous surfactant solution was centrifuged at 1500 rpm to remove unexfoliated crystals. The supernatant liquid was collected and then used as the starting dispersion for the next cascade. This dispersion mainly contained nanosheets of different thickness (expressed as different numbers of monolayers per nanosheet) and a small proportion of single-layer nanosheets with nontrivial lateral size distribution.[82]

The starting dispersion was centrifuged at 2000 rpm. The sediment contained the largest nanoparticles while the supernatant liquid contained smaller ones. The sediment was conditionally referred to as the sample '1.5 – 2 krpm'. It was dispersed in water containing a surfactant (0.1 g litre^{-1}). The supernatant was centrifuged at 3000 rpm and the sediment was referred to as the sample '2 – 3 krpm'. In each step of the cascade centrifugation the dispersion was enriched in single-layer nanosheets. Measurements for nanosheets from all fractions revealed a decrease in their lateral size and thickness with increasing the centrifugation rate. The process was terminated at 10 000 rpm since in this case

the supernatant liquid contained the surfactant and ultrasmall WS_2 nanosheets.[82]

The cascade is designed according to the goal. Experiments described in the preceding paragraph were aimed to fractionate the starting dispersion in such a manner that each subsequent fraction should contain smaller-size nanosheets. If a specific nanoparticle size distribution is necessary, one can use two appropriate rotation speed.[82]

Nanosheets from each fraction were studied by TEM and AFM. After the seventh cascade the ratio of the number of single-layer nanosheets to the total number of nanosheets was equal to 0.4. The length, width and thickness of nanosheets decreased from one fraction to another with increasing rotation speed, the average length and thickness of nanosheets decreases nearly identically, *i.e.*, to a first approximation nanosheets were mass separated. However, a detailed analysis showed that the mechanism of separation of nanosheets by centrifugation is mainly sensitive to the lateral size rather than the mass of nanosheets. For instance, the final fraction of the cascade centrifugation contained a single-layer and a four-layer nanosheets with close lateral size.[82]

The profile of the optical extinction spectrum depends strongly on the size of nanosheets due to the influence of the edge and confinement effects, as was observed earlier for molybdenum disulfide[134] and WS_2. The extinction spectra were measured for nanosheets from all fractions obtained by cascade centrifugation. The size of nanosheets from all fractions was determined by TEM and AFM. The extinction coefficients were calculated using the experimentally measured masses of the dispersed nanoparticles.

The extinction spectra of WS_2 nanosheets demonstrated a single *A*-exciton peak. The position, width and height of this peak varied from one fraction to another depending on the size and thickness of nanosheets and thus in accordance with the edge and confinement effect. The scattering coefficient appeared to be very small; that is why the extinction and absorption coefficients were only slightly different from each other.

It was found that the extinction coefficient depends strongly on the length of nanosheets at all excitation wavelengths except 235 nm. Therefore, the extinction coefficient at 235 nm can be used to determine the concentration of WS_2. The influence of the edge effect on the shape of the extinction spectrum of WS_2 was evaluated using the expression[82]

$$\frac{\mathrm{Ext}_{235}}{\mathrm{Ext}_{290}} = \frac{\alpha_C(235)L_e + 2x(k+1)\Delta\alpha(235)}{\alpha_C(290)L_e + 2x(k+1)\Delta\alpha(290)} \quad (14)$$

where α_C is the absorption coefficient associared with the nanosheet basal plane; $\Delta\alpha = \alpha_E - \alpha_C$, where α_E is the edge-region absorption coefficient; L_e, x and k are respectively the nanosheet length, edge thickness and the nanosheet aspect ratio. Then one has

$$L = \frac{2.3 - \mathrm{Ext}_{235}/\mathrm{Ext}_{290}}{0.02\,\mathrm{Ext}_{235}/\mathrm{Ext}_{290} - 0.0185} \quad (15)$$

where L is the nanosheet length in nanometres and Ext_{235} and Ext_{290} are the dispersion extinction intensities at 235 and 290 nm, respectively. The 290 nm wavelength was chosen arbitrarily since this is the wavelength at which all fractions of the cascade were characterized by different extinction coefficients. The extinction spectra allow one to evaluate the thickness of nanosheets associated with the confinement effect, *viz.*, the smaller the number of layers in the nanosheet the larger the hypsochromic (blue) shift of the *A*-exciton position in the spectra. An empirical equation was proposed[82]

$$\langle N \rangle = 6.35 \times 10^{-32} \mathrm{e}^{\lambda_A/8.51} \quad (16)$$

where N is the number of layers per nanosheet, λ_A is the *A*-exciton wavelength in nanometres. However, it was found that the magnitude of the shift of the *A*-exciton also depends on the dispersion medium. For aqueous solutions of surfactants and *N*-methyl-2-pyrrolidone the positions of the *A*-exciton peaks in the spectra differ by 1.5 nm.

Since only single-layer nanosheets exhibit photoluminescence (for WS_2 a typical peak is at 612 nm), one can determine the content of single-layer nanosheets using a combination of the photoluminescence and Raman spectra. The intensity of the Raman spectrum is proportional to the concentration of WS_2 crystals of any thickness; therefore, the ratio of the fluorescence intensity to the Raman spectrum intensity is a linear function of the volume fraction of single-layer nanosheets. The spectra were normalized to the one of Raman modes.[82]

This dependence was confirmed experimentally for nanosheets with a broad lateral size distribution, but not for the smallest nanosheets for which the edge effects seem to be responsible for strong nonradiative scattering of the excitation energy.

To obtain a maximum proportion of single-layer nanosheets, size-selected dispersions should be centrifuged for 24 h at relatively low speed to remove multilayer nanosheets and then the supernatant liquid should be isolated and short-time (1–4 h) centrifuged at high speed to isolate the remaining small nanosheets; in this case, the sediment contains single-layer nanosheets.[82]

Cascade centrifugation treatment of MoS_2 and WS_2 crystals requires thorough preliminary preparation to fit the method to each substance, but this makes the technique of great value for operation with different batches of raw materials in production.

10. Conclusion

From the aforesaid it follows that no versatile exfoliation procedure has been developed so far. Usually, the yields of exfoliation are low, whereas the energy expenditure and materials consumption are rather high. However, prospects for the design of novel materials with unique properties are so promising that improvement of methods of exfoliation will inevitably continue with high intensity.

The last 15 years were marked by great efforts made to explore methods of exfoliation as well as to study the properties and to find potential fields of practical application of nanosheets of various chemical compounds. The starting point was the preparation of graphene nanosheets using Scotch tape (the technique is still alive), while the last two or three years demonstrate progress in the development of technology for mass production of nanosheets and methods of size control in

flow systems, suitable for large-scale applications. Researchers have paid attention to osmotic swelling, a useful method applicable to aqueous and organic dispersions. Exfoliation in ILs and in supercritical fluids offer great promise in the case of hydrophobic substances, although they are more expensive than osmotic swelling. Electrochemical exfoliation techniques have potentially high yields, are relatively cheap and thus also have a great potential.

The available methods of exfoliation of crystals are characterized by low yield of single-layer nanosheets. This makes the search for more efficient methods topical. At present, it is clear that obtaining maximum proportion of single-layer nanosheets requires grinding of crystals since the smaller the lateral size the smaller the thickness of nanosheets. On the other hand, the smaller the nanosheet the larger the total edge length; note that edge effects have strong impact on, *e.g.*, catalytic properties of nanosheets.

Undoubtedly, further improvement of methods for size selection of exfoliated nanosheets is necessary. The available methods are labour-, energy-, material- and time-consuming. This gives an impetus to the development of novel methods for separation of nanosheets. This avenue of research seems to be particularly promising in connection with rapid progress in the design of hybrid materials combining nanosheets and the 0D or 1D nanocrystals that not only act as stabilizers, but also produce a synergistic effect on the functional properties of the novel materials.

The authors express their gratitude to A.S.Bushmeleva and V.N.Zakharov for help in the preparation of the Figures for publication.

This review has been written with the financial support from the Russian Foundation for Basic Research (Project No. 15-03-06948).

Figures 2, 3, 4, 6, 7 and 8 are courtesy of The American Chemical Society.

Figure 5 is courtesy of Sociedade Brasileira de Quimica.

Figure 9 is courtesy of John Wiley and Sons.

Figure 11 is courtesy of Elsevier.

Figure 12 is courtesy of Springer Nature.

References

1. P.Joensen, R.F.Frindt, S.R.Morrison. *Mater. Res. Bull.*, **21**, 457 (1986)
2. D.W.Murphy, G.W.Hull Jr. *J. Chem. Phys.*, **62**, 973 (1975)
3. A.Usuki, Y.Kojima, M.Kawasumi, A.Okada, Y.Fukushima, T.Kurauchi, O.Kamigaito. *J. Mater. Res.*, **8**, 1179 (1993)
4. Y.Kojima, A.Usuki, M.Kawasumi, A.Okada, Y.Fukushima, T.Kurauchi, O.Kamigaito. *J. Mater. Res.*, **8**, 1185 (1993)
5. A.Okada, A.Usuki. *Macromol. Mater. Eng.*, **291**, 1449 (2006)
6. A.Dasari, G.-P.Cai, Y.-W.Mai, Z.-Z.Yu, in *Physical Properties and Applications of Polymer Nanocomposites*. (Eds S.C.Tjong, Y.-W.Mai). (Oxford, Cambridge, Philadelphia, New Delhi, 2010). P. 347
7. Y.Cui, S.Kumar, B.R.Kona, D.van Houcke. *RSC Adv.*, **5**, 63669 (2015)
8. D.Cai, M.Song. *J. Appl. Polym. Sci.*, **132**, 41314 (2015)
9. S.W.Kim, S.-H.Cha. *J. Appl. Polym. Sci.*, **131**, 40289 (2014)
10. A.V.Murugan, T.Muraliganth, A.Manthiram. *Chem. Mater.*, **21**, 5004 (2009)
11. G.Chen, C.Wu, W.Weng, D.Wu, W.Yan. *Polymer*, **44**, 1781 (2003)
12. K.S.Novoselov, A.K.Geim, S.V.Morozov, D.Jiang, Y.Zhang, S.V.Dubonos, I.V.Grigorieva, A.A.Firsov. *Science*, **306**, 666 (2004)
13. T.Sasaki, M.Watanabe, H.Hashizume, H.Yamada, H.Nakazawa. *J. Am. Chem. Soc.*, **118**, 8329 (1996)
14. C.Toumey. *Nat. Nanotechnol.*, **11**, 2 (2016)
15. Q.H.Wang, K.Kalantar-Zadeh, A.Kis, J.N.Coleman, M.S.Strano. *Nat. Nanotechnol.*, **7**, 699 (2012)
16. O.N.Weiss, H.Zhou, L.Liao, Y.Liu, S.Jiang, Y.Huan, X.Duan. *Adv. Mater.*, **24**, 5782 (2012)
17. B.Radisavljevic, A.Radenovic, J.Brivio, V.Giacometti, A.Kis. *Nat. Nanotechnol.*, **6**, 147 (2011)
18. L.Li, Y.Yu, G.J.Ye, Q.Ge, X.Ou, H.Wu, D.Feng, X.H.Chen, Y.Zhang. *Nat. Nanotechnol.*, **9**, 372 (2014)
19. H.Liu, A.T.Neal, Z.Zhu, Z.Luo, X.Xu, D.Tomanek, P.D.Ye. *ACS Nano*, **8**, 4033 (2014)
20. F.Xia, H.Wang, Y.Jia. *Nat. Commun.*, **5**, 4458 (2014)
21. A.Pakdel, Y.Bando, D.Golbery. *Chem. Soc. Rev.*, **43**, 934 (2014)
22. D.Xiao, G.-B.Liu, W.Feng, X.Xu, W.Yao. *Phys. Rev. Lett.*, **108**, 196802 (2012)
23. L.Britnell, R.V.Gorbachev, R.Jalil, B.D.Belle, F.Schedin, A.Mishchenko, T.Georgiou, M.I.Katsnelson, L.Eaves, S.V.Morozov, N.M.R.Peres, J.Leist, A.K.Geim, K.S.Novoselov, L.A.Ponomarenko. *Science*, **335**, 947 (2012)
24. L.Chen, K.Sun, P.Li, X.Fan, J.Sun, S.Ai. *Nanoscale*, **5**, 10982 (2013)
25. F.Ji, X.Ren, X.Zheng, Y.Liu, L.Pang, J.Jiang, S.F.Liu. *Nanoscale*, **8**, 8696 (2016)
26. P.F.Liu, S.Yang, B.Zhang, H.G.Yang. *ACS Appl. Mater. Interfaces*, **8**, 34474 (2016)
27. L.-R.Zou, G.-F.Huang, D.-F.Li, J.-H.Liu, A.-L.Pan, W.-Q.Huang. *RSC Adv.*, **6**, 86688 (2016)
28. L.Zhang, C.Li, D.Jiang, T.Feng, Q.Li. *Key Eng. Mater.*, **544**, 259 (2013)
29. X.Zhang, X.Xie, H.Wang, J.Zhang, B.Pan, Y.Xie. *J. Am. Chem. Soc.*, **135**, 18 (2013)
30. L.Zhou, Y.Xu, W.Yu, X.Guo, S.Yu, J.Zhang, C.Li. *J. Mater. Chem., A*, **4**, 8000 (2016)
31. D.Er, J.Li, M.Nagui, Y.Gogotsi, V.B.Shenoy. *ACS Appl. Mater. Interfaces*, **6**, 11173 (2014)
32. H.Jang, S.Suzuki, M.Miyayama. *J. Power Sources*, **203**, 97 (2012)
33. S.-Y.Lin, X.Zhang. *J. Power Sources*, **294**, 354 (2015)
34. D.Hanlon, C.Backes, T.Higgins, J.M.Hughes, A.O'Neill, P.J.King, N.McEvoy, G.S.Duesberg, B.Mendoza-Sanchez, H.Pettersson, V.Nicolosi, J.N.Coleman. *Chem. Mater.*, **26**, 1751 (2014)
35. X.Zhang, M.Xue, X.Yang, Z.Wang, G.Luo, Z.Huang, X.Sui, C.Li. *RSC Adv.*, **5**, 2762 (2015)
36. F.Torrisi, J.N.Coleman. *Nat. Nanotechnol.*, **9**, 738 (2014)
37. P.A.Hu, Z.Wen, L.Wang, P.Tan, K.Xiao. *ACS Nano*, **6**, 5988 (2012)
38. M.Laurenti, A.E.A.Subaie, M.-N.Abdallah, A.R.G.Cortes, J.L.Ackerman, H.Vali, K.Basu, Y.L.Zhang, M.Murshed, S.Strandman, J.X.X.Zhu, N.Makhoul, J.E.Barralet, F.Tamimi. *Nano Lett.*, **16**, 4779 (2016)
39. E.D.Grayfera, M.N.Kozlova, V.E.Fedorov. *Adv. Colloid Interface Sci.*, **245**, 40 (2017)

40. Y.Song, W.Fang, R.Brenes, J.Kong. *Nano Today*, **10**, 681 (2015)
41. F.Wang, Z.Wang, Q.Wang, F.Wang, L.Yin, K.Xu, Y.Huang, J.He. *Nanotechnology*, **26**, 292001 (2015)
42. S.J.McDonnell, R.M.Wallace. *Thin Solid Films*, **616**, 482 (2016)
43. A.Castellanos-Gomez. *J. Phys. Chem. Lett.*, **6**, 4280 (2015)
44. L.A.Aslanov, G.V.Fetisov, K.A.Paseshnichenko, S.F.Dunaev. *Coord. Chem. Rev.*, **352**, 220 (2017)
45. H.Li, J.Wu, Z.Yin, H.Zhang. *Acc. Chem. Res.*, **47**, 1067 (2014)
46. A.Castellanos-Gomez, E.Navarro-Moratalla, G.Mokry, J.Quereda, E.Pinilla-Cienfuegos, N.Agraït, H.S.J.van der Zant, E.Coronado, G.A.Steele, G.Rubio-Bollinger. *Nano Res.*, **6**, 191 (2013)
47. J.O.Island, M.Barawi, R.Biele, A.Almazán, J.M.Clamagirand, J.R.Ares , C.Sánchez, H.S.J.van der Zant, J.V.Álvarez, R.D'Agosta, I.J.Ferrer, A.Castellanos-Gomez. *Adv. Mater.,* **27**, 2595 2015
48. M.Bialoglowski, C.Jastrzebski, S.Podsiadlo, D.J.Jastrzebski, R.Gajda, W.Gebicki, P.A.Wrzosek, K.Wozniak. *Cryst. Res. Technol.*, **50**, 695 (2015)
49. F.A.S.Al-Alamy, A.A.Balchin, M.White. *J. Mater. Sci.*, **12**, 2037 (1977).
50. B.Paosz, W.Paosz, S.Gierlotka. *Acta Crystallogr., Sect. C*, **41**, 807 (1985)
51. B.Paosz, W.Steurer, H.Schultz. *Acta Crystallogr., Sect. B*, **46**, 449 (1990)
52. P.Wahnon, J.C.Conesa, P.Palacios, R.Lucena, I.Aguilera, Y.Seminovski, F.Fresno. *Phys. Chem. Chem. Phys.*, **13**, 20401 (2011)
53. J.Dong, C.Li, J.Yang, B.Chen, H.Song, J.Chen, W.Peng. *Cryst. Res. Technol.*, **51**, 671 (2016)
54. H.Shalchian, J.V.Khaki, A.Babakhani, G.Taglieri, I.De Michelis, V.Daniele, F.Veglio. *Ceram. Intern.*, **43**, 12957 (2017)
55. J.Ji, J.Wen, Y.Shen, Y.Lv, Y.Chen, S.Liu, H.Ma, Y.Zhang. *J. Am. Chem. Soc.*, **139**, 11698 (2017)
56. C.Backes, T.M.Higgins, A.Kelly, C.Boland, A.Harvey, D.Hanlon, J.N.Coleman. *Chem. Mater.*, **29**, 243 (2017)
57. C.Backes, N.C.Berner, X.Chen, P.Lafargue, P.LaPlace, M.Freeley, G.S.Duesberg, J.N.Coleman, A.R.McDonald. *Angew. Chem., Int. Ed.*, **54**, 2638 (2015)
58. G.Cunningham, M.Lotya, C.S.Cucinotta, S.Sanvito, S.D.Bergin, R.Menzel, M.S.P.Shaffer, J.N.Coleman. *ACS Nano*, **6**, 3468 (2012)
59. A.Ciesielski, P.Samori. *Chem. Soc. Rev.*, **43**, 381 (2014)
60. J.N.Coleman, M.Lotya, A.O'Neill, S.D.Bergin, P.J.King, U.Khan, K.Young, A.Gaucher, S.De, R.J.Smith, I.V.Shvets, S.K.Arora, G.Stanton, H.-Y.Kim, K.Lee, G.T.Kim, G.S.Duesberg, T.Hallam, J.J.Boland, J.J.Wang, J.F.Donegan, J.C.Grunlan, G.Moriarty, A.Shmeliov, R.J.Nicholls, J.M.Perkins, E.M.Grieveson, K.Theuwissen, D.W.McComb, P.D.Nellist, V.Nicolosi. *Science*, **331**, 568 (2011)
61. W.Du, X.Jiang, L.Zhu. *J. Mater. Chem. A*, **1**, 10592 (2013)
62. Y.Hernandez, V.Nicolosi, M.Lotya, F.M.Blighe, Z.Sun, S.De, I.T.McGovern, B.Holland, M.Byrne, Y.K.Gun Ko, J.J.Boland, P.Niraj, G.Duesberg, S.Krishnamurthy, R.Goodhue, J.Hutchison, V.Scardaci, A.C.Ferrari, J.N.Coleman. *Nat. Nanotechnol.*, **3**, 563 (2008)
63. V.Nicolosi, M.Chhowalla, M.G.Kanatzidis, M.S.Strano, J.N.Coleman. *Science*, **340**, 1420 (2013)
64. K.Parvez, Z.Wu, R.Li, X.Liu, R.Graf, X.Feng, K.Müllen. *J. Am. Chem. Soc.*, **136**, 6083 (2014)
65. K.R.Paton, E.Varrla, C.Backes, R.J.Smith, U.Khan, A.O'Neill, C.Boland, M.Lotya, O.M.Istrate, P.King, T.Higgins, S.Barwich, P.May, P.Puczkarski, I.Ahmed, M.Moebius, H.Pettersson, E.Long, J.Coelho, S.E.O'Brien, E.K.McGuire, B.M.Sanchez, G.S.Duesberg, N.McEvoy, T.J.Pennycook, C.Downing, A.Crossley, V.Nicolosi, J.N.Coleman. *Nat. Mater.*, **13**, 624 (2014)
66. E.Varrla, C.Backes, K.R.Paton, A.Harvey, Z.Gholamvand, J.McCauley, J.N.Coleman. *Chem. Mater.*, **27**, 1129 (2015)
67. J.Shen, Y.He, J.Wu, C.Gao, K.Keyshar, X.Zhang, Y.Yang, M.Ye, R.Vajtai, J.Lou, P.M.Ajayan. *Nano Lett.*, **15**, 5449 (2015)
68. B.J.Carey, T.Daeneke, E.P.Nguyen, Y.Wang, J.Zhen, S.Zhuiykov, K.Kalantar-zadeh. *Chem. Commun.*, **51**, 3770 (2015)
69. U.Halim, C.R.Zheng, Y.Chen, Z.Lin, S.Jiang, R.Cheng, Y.Huang, X.Duan. *Nat. Commun.*, **4**, 3213 (2013)
70. K.Zhou, N.Mao, H.Wang, Y.Peng, H.Zhang. *Angew. Chem., Int. Ed.*, **50**, 10839 (2011)
71. Y.Nonomura, Y.Morita, S.Deguchi, S.Mukai. *J. Colloid Interface Sci.*, **346**, 96 (2010)
72. M.Yi, Z.Shen, S.Ma, X.Zhang. *J. Nanopart. Res.*, **14**, 1003 (2012)
73. M.Yi, Zh.Shen, X.Zang, Sh.Ma. *J. Phys. D*, **46**, 025301 (2013)
74. J.Shen, J.Wu, M.Wang, P.Dong, J.Xu, X.Li, X.Zhang, J.Yuan, X.Wang, M.Ye, R.Vajtai, J.Lou, P.M.Ajayan. *Small*, **12**, 2741 (2016)
75. G.Li, L.Li, H.Yuan, H.Wang, H.Zeng, J.Shi. *J. Colloid Interface Sci.*, **495**, 19 (2017)
76. L.Niu, J.N.Coleman, H.Zhang, H.Shin, M.Chhowalla, Z.Zheng. *Small*, **12**, 272 (2016)
77. D.Wang, F.Wu, Y.Song, C.Li, L.Zhou. *J. Alloys Compd.*, **728**, 1030 (2017)
78. W.Luo, Y.Wang, E.Hitz, Y.Lin, B.Yang, L.Hu. *Adv. Funct. Mater.*, **27**, 1701450 (2017)
79. E.Varrla, K.R.Paton, C.Backes, A.Harvey, R.J.Smith, J.McCauley, J.N.Coleman. *Nanoscale*, **6**, 11810 (2014)
80. L.Niu, M.Li, X.Tao, Z.Xie, X.Zhou, A.P.A.Raju, R.J.Young, Z.Zheng. *Nanoscale*, **5**, 7202 (2013)
81. L.Niu, K.Li, H.Zhen, Y.-S.Chui, W.Zhang, F.Yan, Z.Zheng. *Small*, **10**, 4651 (2014)
82. C.Backes, B.M.Szydlowska, A.Harvey, S.Yuan, V.Vega-Mayoral, B.R.Davies, P.-L.Zhao, D.Hanlon, E.Santos, M.I.Katsnelson, W.J.Blau, C.Gadermaier, J.N.Coleman. *ACS Nano*, **10**, 1589 (2016)
83. F.Geng, R.Ma, A.Nakamura, K.Akatsuka, Y.Ebina, Y.Yamauchi, N.Miyamoto, Y.Tateyama, T.Sasaki. *Nat. Commun.*, **4**, 1632 (2013)
84. T.Maluangnont, K.Matsuba, F.Geng, R.Ma, Y.Yamauchi, T.Sasaki. *Chem. Mater.*, **25** 3137 (2013)
85. F.Geng, R.Ma, Y.Ebina, Y.Yamauchi, N.Miyamoto, T.Sasaki. *J. Am. Chem. Soc.*, **136**, 5491 (2014)
86. F.Geng, R.Ma, Y.Yamauchi, T.Sasaki. *Chem. Commun.*, **50**, 9977 (2014)
87. T.Sasaki, M.Watanabe. *J. Am. Chem. Soc.*, **120**, 4682 (1998)
88. T.Tanaka, Y.Ebina, K.Takada, K.Kurashima, T.Sasaki. *Chem. Mater.*, **15**, 3564 (2003)
89. Z.Liu, R.Ma, Y.Ebina, K.Takada, T.Sasaki. *Chem. Mater.*, **19**, 6504 (2007)
90. Z.-H.Liu, K.Ooi, H.Kanoh, W.-P.Tang, T.Tomida. *Langmuir*, **16**, 4154 (2000)
91. Y.Omomo, T.Sasaki, L.Z.Wang, M.Watanabe. *J. Am. Chem. Soc.*, **125**, 3568 (2003)

92. X.Yang, Y.Makita, Z.-H.Liu, K.Sakane, K.Ooi. *Chem. Mater.*, **16**, 5581 (2004)
93. Y.Cui, Z.-H.Liu, M.Wang, K.Ooi. *Chem. Lett.*, **35**, 740 (2006)
94. A.L.Shiguihara, M.A.Bizeto, V.R.L.Constantino. *J. Braz. Chem. Soc.*, **21**, 1366 (2010)
95. Z.Liu, R.Ma, M.Osada, N.Iyi, Y.Ebina, K.Takada, T.Sasaki. *J. Am. Chem. Soc.*, **128**, 4872 (2006)
96. A.Kuhn, T.Holzmann, J.Nuss, B.V.Lotsch. *J. Mater. Chem., A*, **2**, 6100 (2014)
97. H.Yuan, D.Dubbink, R.Besselink, J.E.ten Elshof. *Angew. Chem., Int. Ed.*, **54**, 9239 (2015)
98. J.Connolly, J.S.van Duijneveldt, S.Klein, C.Pizzey, R.M.Richardson. *Langmuir*, **22**, 6531 (2006)
99. R.Besselink, T.M.Stawski, H.L.Castricum, D.H.A.Blank, J.E.ten Elshof. *J. Phys. Chem. C*, **114**, 21281 (2010)
100. 1A.A.Jeffery, A.Pradeep, M.Rajamathi. *Phys. Chem. Chem. Phys.*, **18**, 12604 (2016)
101. M.R.Allen, A.Thibert, E.M.Sabio, N.D.Browning, D.S.Larsen, F.E.Osterloh. *Chem. Mater.*, **22**, 1220 (2010)
102. D.Li, J.Yang, L.Zhang, X.Wang, L.Lu, X.Yang. *J. Mater. Chem.*, **12**, 1796 (2002)
103. L.Wang, T.Sasaki. *Chem. Rev.*, **114**, 9455 (2014)
104. L.Ren, X.Qi, Y.Liu, G.Hao, Z.Huang, X.Zou, L.Yang, J.Li, J.Zhong. *J. Mater. Chem.*, **22**, 4921 (2012)
105. C.Zang, X.Qi, L.Ren, G.Hao, Y.Liu, J.Li, J.Zhong. *Appl. Surface Sci.*, **316**, 341 (2014)
106. X.Ren, X.Qi, Y.Shen, G.Xu, J.Li, Z.Li, Z.Huang, J.Zhong. *Mater. Sci. Eng. B*, **214**, 46 (2016)
107. H.Ju, J.Kim. *Chem. Eng. J.*, **297**, 66 (2016)
108. H.Ju, J.Kim. *ACS Nano*, **10**, 5730 (2016)
109. U.Sen, K.K.Kundu, M.N.Das. *J. Phys. Chem.*, **71**, 3665 (1967)
110. S.S.Chou, M.De, J.Kim, S.Byun, C.Dykstra, J.Yu, J.Huang, V.P.Dravid. *J. Am. Chem. Soc.*, **135**, 4584 (2013)
111. G.Eda, H.Yamaguchi, D.Voiry, T.Fujita, M.Chen, M.Chhowalla. *Nano Lett.*, **11**, 5111 (2011)
112. G.Eda, T.Fujita, H.Yamaguchi, D.Voiry, M.Chen, M.Chhowalla. *ACS Nano*, **6**, 7311 (2012)
113. Z.Zeng, Z.Yin, X.Huang, H.Li, Q.He, G.Lu, F.Boey, H.Zhang. *Angew. Chem., Int. Ed.*, **50**, 11093 (2011)
114. J.Peng, J.Wu, X.Li, Y.Zhou, Z.Yu, Y.Guo, J.Wu, Y.Lin, Z.Li, X.Wu, C.Wu, Y.Xie. *J. Am. Chem. Soc.*, **139**, 9019 (2017)
115. C.Guo, H.Li, W.Zhao, J.Pan, T.Lin, J.Xu, M.Chen, F.Huang. *J. Mater. Chem. C*, **5**, 5977 (2017)
116. N.Liu, P.Kim, J.H.Kim, J.H.Ye, S.Kim, C.J.Lee. *ACS Nano*, **8**, 6902 (2014)
117. A.Ambrosi, Z.Sofer, M.Pumera. *Angew. Chem., Int. Ed.*, **56**, 10443 (2017)
118. T.Daeneke, R.M.Clark, B.J.Carey, J.Z.Ou, B.Weber, M.S.Fuhrer, M.Bhaskaran, K.Kalantar-zadeh. *Nanoscale*, **8**, 15252 (2016)
119. R.M.Clark, J.C.Kotsakidis, B.Weber, K.J.Berean, B.J.Carey, M.R.Field, H.Khan, J.Z.Ou, T.Ahmed, C.J.Harrison, I.S.Cole, K.Latham, K.Kalantar-zadeh, T.Daeneke. *Chem. Mater.*, **28**, 8942 (2016)
120. J.Zheng, H.Zhang, S.Dong, Y.Liu, C.T.Nai, H.S.Shin, H.Y.Jeong, B.Liu, K.P.Loh. *Nat. Commun.*, **5**, 2995 (2014)
121. T.E.Sutto, T.T.Duncan. *Electrochim. Acta*, **77**, 204 (2012)
122. G.Kamath, G.A.Baker. *RSC Adv.*, **3**, 8197 (2013)
123. E.Darve, A.Pohorille. *J. Chem. Phys.*, **115**, 9169 (2001)
124. G.Kamath, G.A.Baker. *Phys. Chem. Chem. Phys.*, **14**, 7929 (2012)
125. T.Fukushima, T.Aida. *Chem. – Eur. J.*, **13**, 5048 (2007)
126. T.Ludwig, L.Guo, P.McCrary, Z.Zhang, H.Gordon, H.Quan, M.Stanton, R.M.Frazier, R.D.Rogers, H.-T.Wang, C.H.Turner. *Langmuir*, **31**, 3644 (2015)
127. A.Abedini, T.Ludwig, Z.Zhang, C.H.Turner. *Langmuir*, **32**, 9982 (2016)
128. X.Zhang, S.Heinonen, E.Levanen. *RSC Adv.*, **4**, 61137 (2014)
129. Y.Wang, C.Zhou, W.Wang, Y.Zhao. *Ind. Eng. Chem. Res.*, **52**, 4379 (2013)
130. G.Hu, L.Yi, C.Liu. *J. Supercrit. Fluids*, **72**, 59 (2012)
131. C.Liu, G.Hu. *RSC Adv.*, **3**, 20877 (2013)
132. J.Kang, J.-W.T.Seo, D.Alducin, A.Ponce, M.J.Yacaman, M.C.Hersam. *Nat. Commun.*, **5**, 5478 (2014)
133. A.A.Greenand, M.C.Hersam. *Nano Lett.*, **9**, 4031, 2009
134. C.Backes, R.J.Smith, N.McEvoy, N.C.Berner, D.McCloskey, H.C.Nerl, A.O'Neill, P.J.King, T.Higgins, D.Hanlon, N.Scheuschner, J.Maultzsch, L.Houben, G.S.Duesberg, J.F.Donegan, V.Nicolosi, J.N.Coleman. *Nat. Commun.*, **5**, 4576 (2014)
135. K.Dolui, C.D.Pemmaraju, S.Sanvito. *ACS Nano*, **6**, 4823 (2012)
136. H.R.Gutieírrez, N.Perea-López, A.L.Elías, A.Berkdemir, B.Wang, R.Lv, F.López-Urías, V.H.Crespi, H.Terrones, M.Terrones. *Nano Lett.*, **13**, 3447 (2013)